TORSIONAL VIBRATION ANALYSIS AND TESTING OF SYNCHRONOUS MOTOR-DRIVEN TURBOMACHINERY

by

Mark A. Corbo

President and Chief Engineer

No Bull Engineering

Delmar, New York

Clifford P. Cook

Texaco Fellow

ChevronTexaco, Inc.

Houston, Texas

Charles W. Yeiser

Principal Engineer

Rotor Bearing Technology & Software, Inc.

Phoenixville, Pennsylvania

and

Michael J. Costello

Senior Specialist

ChevronTexaco, Inc.

Houston, Texas

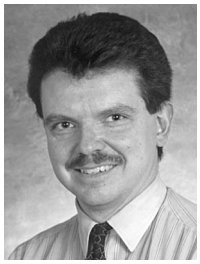

Mark A. Corbo is President and Chief Engineer of No Bull Engineering, a high technology engineering/consulting firm, in Delmar, New York. He is responsible for rotating equipment consulting services in the forms of engineering design and analysis, troubleshooting, and third-party design audits. Before beginning his consulting career at MTI in 1995, he spent 12 years in the aerospace industry designing pumps, valves, and controls for gas turbine engines. His expertise includes rotordynamics, fluid-film journal and thrust bearings, dynamic simulations, hydraulic and pneumatic flow analysis, CFD, FEA, and mechanical design.

Mr. Corbo has B.S. and M.S. degrees (Mechanical Engineering) from Rensselaer Polytechnic Institute. He is a registered Professional Engineer in the State of New York, and is a member of ASME, STLE, and The Vibration Institute. He has authored more than a dozen technical publications, including one that won the "Best Case Study" award at Bently Nevada's ISCORMA conference in 2001.

Clifford P. (Cliff) Cook is with ChevronTexaco, Inc., in Houston, Texas. He is Chairman of the API RP 687 Task Force on Repair of Special Purpose Rotors. He is a Texaco Fellow, registered Professional Engineer in the State of Texas, Chairman of the API Subcommittee on Mechanical Equipment, and a member of the Texas A&M Turbomachinery Symposium Advisory Committee. Mr. Cook is a member of API 617 (compressors), 613 (SP gears), 677 (GP gears), 616 (gas turbines), and past member of API 684 (rotordynamics tutorial), 610 (pumps), 618 (reciprocating compressors) task forces.

Mr. Cook has a B.S. degree from the U.S. Merchant Marine Academy, Kings Point, and an M.S. degree (Mechanical Engineering) from Lehigh University.

Charles W. Yeiser is a Principal Engineer at Rotor Bearing Technology & Software, Inc. (RBTS), in Phoenixville, Pennsylvania—a software and consulting services company specializing in rotating systems. His responsibilities include modeling, analyzing, and measuring the performance of rotating systems. He has been extensively involved in the development and implementation of computational solution algorithms related to rotordynamics, torsional vibration, and fluid-film/rolling element bearings. Prior to working at RBTS, Mr. Yeiser was employed by the Franklin Research Center (formerly the Franklin Institute Research Laboratories) as a Mechanical Engineer. His fields of expertise include torsional vibration, rolling element bearings, rotordynamics, finite element analysis, and customized field test/sensor development (strain gauges, proximity probes, accelerometers, data acquisition, etc.).

Mr. Yeiser has a B.A. degree (Physics) from Franklin and Marshall College, and B.S. and M.S. degrees from the University of Pennsylvania. He has authored numerous technical reports and papers for private industry and government agencies.

ABSTRACT

One of the foremost concerns facing turbomachinery users today is that of torsional vibration. In contrast to lateral rotordynamics problems, torsional failures are especially heinous since the first

symptom of a problem is often a broken shaft, gear tooth, or coupling. The difficulty of detecting incipient failures in the field makes the performance of a thorough torsional vibration analysis an essential component of the turbomachinery design process.

The primary objective of this tutorial is to provide such a procedure for the special case where the turbomachine is driven by a synchronous motor. Synchronous motors are one of the most notorious sources of torsional vibration problems because of the large pulsating torques they generate during startups. The torsional shaft stresses generated by these large pulsations are usually greater than the shaft material endurance limits, thereby, causing the lives of such machines to be limited.

The determination of the number of startups that these machines can survive is, therefore, a critical portion of their design process. It is the authors' experience that there is a great deal of confusion over the proper way to do this. The full impact of this confusion was seen on a recently designed compressor train where the use of one method showed the allowable number of starts to be zero while a second procedure predicted infinite life. In an attempt to alleviate this confusion, a logical, step-by-step procedure, based on the strain-life theory of failure, was generated and is presented herein. An example illustrating how the authors used this procedure to design a critical 66,000 hp air compressor is also presented. The authors believe that employment of this method may well save the user from the need to introduce an expensive and unwieldy Holset-style damping coupling into some future compressor train.

Although the presented analytical procedure is quite rigorous, there are cases, especially on critical equipment, where it is wise to augment its predictions with torsional test data taken from the field. The best way to do this in synchronous motor-driven equipment is to apply strain gauges to critical shafts in the drive train and measure the actual torques that are generated during startup. Accordingly, a general description of strain gauge testing fundamentals is provided to familiarize all users with it. Additionally, the use of this valuable testing procedure is illustrated via the same 66,000 hp air compressor that was used to illustrate the analytical procedure. The tutorial closes with a comparison of the obtained analytical and test results and an illustration of how the authors used the testing to "fine-tune" the analytical results.

INTRODUCTION

Torsional vibration is a subject that should be of concern to all turbomachinery users. By some accounts, torsional vibration is the leading cause of failures in turbomachinery drive trains. Some typical effects of uncontrolled torsional vibration are failed couplings, broken shafts, worn gears and splines, and fractured gear teeth. Accordingly, a thorough torsional vibration analysis should be included as an integral part of the turbomachinery design process. A comprehensive procedure for performing this analysis is provided in Corbo and Malanoski (1996).

The criticality of performing this analysis is heightened whenever the system is driven by an AC synchronous motor. Synchronous motors are one of the most notorious sources of torsional vibration problems because of the torque pulsations they produce during startups. Since the magnitudes of these pulsations are usually substantial, the resulting shaft stresses are often above the material endurance limits, making the shafts susceptible to fatigue. Accordingly, there is usually a definite limit to the number of startups that a synchronous motor-driven train can safely be subjected to. It is the aim of this tutorial to provide users with a practical analytical procedure for predicting this limit and to highlight the criticality of proper selection of the factors employed in the analysis.

Because equipment that employs synchronous motors is often highly critical, it is often prudent to supplement the torsional analysis with field testing using strain gauges to validate the system analytical model and determine the relative accuracy of the analytical results. It is, therefore, also an aim of this tutorial to provide users with the fundamentals of strain gauge testing and to give them the knowledge needed to implement such a test program.

The tutorial begins with a brief description of synchronous motors and the mechanisms that make them such a hazard from a torsional vibration standpoint. A step-by-step procedure is then given for calculating the number of starts that a synchronous motor-driven machine can be safely subjected to. The initial steps, generation of a lumped parameter model, calculation of natural frequencies, and generation of Campbell diagrams, are only given a cursory treatment since they are described in detail in other publications. However, the later steps, performance of the time-transient analysis and, especially, determination of the shaft fatigue lives, are treated in detail.

The authors have observed that most of the existing procedures for predicting fatigue life utilize the traditional stress-life theory of failure and the traditional conservative torsional stress safety factor of 2.0. Although the predicted fatigue life and allowable number of starts are highly sensitive to both these factors (due to the log-log nature of the S-N curve), use of this method is acceptable for many machines since it errs on the conservative side.

However, the authors have, on occasion, found the traditional procedure to be too conservative. After performing a considerable amount of research, the authors have developed a more sophisticated procedure that, while still remaining conservative, provides a more accurate assessment of fatigue life. In the new procedure, the traditional stress-life theory is replaced with the strain-life theory of failure, which has consistently been found to be more accurate. Additionally, the authors found justification for using a safety factor less than the traditional 2.0 value. Furthermore, the authors implemented a rigorous method for accounting for surface finish, size, stress concentration, and notch sensitivity effects as functions of life. This is an area that the authors have observed to be a source of considerable confusion for most engineers.

The mechanics of employing the more sophisticated procedure are illustrated on a 66,000 hp air compression train, and its advantages over the traditional method are clearly pointed out. The high sensitivity of the calculated number of starts to the assumed surface finish, size, stress concentration, notch sensitivity, and safety factors is also demonstrated.

Finally, much of the analysis is validated via strain gauge testing on the subject machine. The fundamentals of strain gauge testing are described and their employment for testing the subject drive train is described in detail. The results of the testing are then compared with the analytical results and utilized to "tweak" the analysis to get its predictions to agree with the test results.

SYNCHRONOUS MOTORS

AC synchronous motors are often applied instead of induction motors in applications where induction motor design and construction limitations occur or where higher system power factors and/or machine efficiencies are desired. Unfortunately, these advantages of synchronous motors do not come without a price since, in the authors' experience, synchronous motors are the most notorious source of torsional vibration problems in turbomachinery. The primary reason for this is that synchronous motors generate large sinusoidal pulsating torques that can easily excite torsional vibrations during the startup process.

Pulsating torques are created during starting due to the fact that synchronous motor rotors contain salient poles, which are magnetic protrusions enclosed by field coils. The resulting asymmetry causes the motor's output torque to vary as a function of rotor position. This effect is in direct contrast to pure induction motors, which have symmetric rotors and a generated torque that is fairly independent of rotor location.

Synchronous motors are typically equipped with squirrel-cage (AKA amortisseur) windings that provide starting torque and also provide damping during steady-state running. During starting,

these windings are utilized to accelerate the motor as an induction motor from zero speed to a speed slightly below synchronous speed. Starting is usually performed with no voltage applied to the rotor's field winding. When synchronous speed is approached, DC field voltage is applied and the rotor is pulled into synchronism. The motor's synchronous speed is given by the following equation:

$$N_S = 120 \bullet f_l / N_p \quad (1)$$

where:
N_S = Synchronous speed (rpm)
f_l = Line frequency (Hz)
N_p = Number of poles in motor

Synchronous motors are often modeled as having two axes of symmetry, the direct axis and the quadrature axis. The direct axis refers to a centerline that passes directly through the center of the rotor's poles while the quadrature axis is perpendicular to the direct axis and comprises the interpolar spaces.

The pulsating torque that occurs during startup arises from both rotor geometry variations that repeat once per pole pitch and those that reappear once for every pole pair. The phenomena that directly translate this asymmetry into torque pulsations include the following:

- Magnetic permeance variations, which occur because the salient poles are relatively more easily magnetized at the center of the pole and less easily magnetized at the center of the interpolar space.
- Asymmetry of the main field winding, which encircles only the direct axis and not the quadrature axis.
- Nonuniform bar placement and composition of the amortisseur or damper windings.

Accordingly, as the rotor rotates, the torque varies in a roughly sinusoidal fashion between the limits imposed by the direct axis and quadrature axis torques. The mean value of these two is referred to as the average torque and represents the torque available to provide acceleration to the system's inertias. Superimposed on this torque is a pulsating torque whose magnitude is one-half the difference between the direct and quadrature axis torques. Figure 1 illustrates the various torque components as a function of speed for a hypothetical synchronous motor.

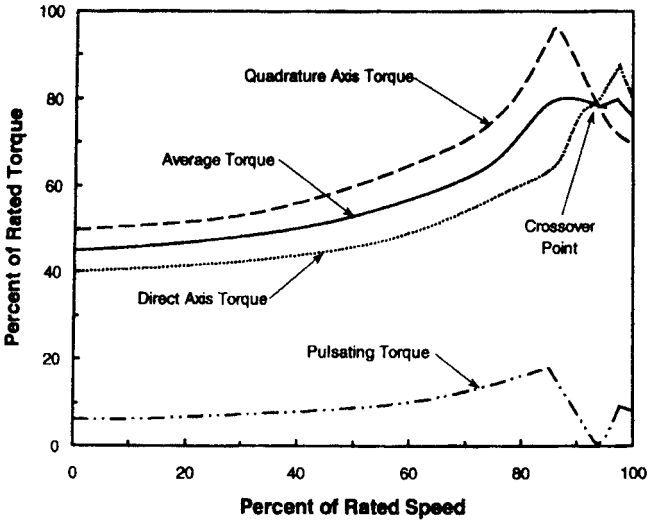

Figure 1. Typical Synchronous Motor Torque-Speed Curve.

The frequency of the torque pulsations is the frequency at which the stator's rotating magnetic field passes a rotor pole. Since the stator's magnetic field rotates at synchronous speed, the excitation frequency is a function of the difference between synchronous speed and rotor speed, which is known as slip speed. The net result of this is a torque pulsation that occurs at twice slip frequency, which is defined by the following equation:

$$f_{slip} = f_l \bullet \left(N_S - N\right) / N_S \quad (2)$$

where:
f_{slip} = Slip frequency (Hz)
f_l = Line frequency (Hz)
N_S = Synchronous speed (rpm)
N = Rotor speed (rpm)

When the main field winding is excited, the electromagnetic geometry repeats once for every two poles and there exists an additional component of continuous torque pulsation at slip frequency. In most cases, the field winding is shorted either across the terminals or through a resistor. If the motor accelerates without the field excitation already applied, the frequency of the pulsating torque then varies nearly linearly from twice the line frequency at standstill to zero frequency at synchronous speed. However, should the field excitation be applied before synchronizing speed is reached, an additional large component of pulsating torque appears with a frequency equal to one-half the original component (i.e., at the slip frequency).

The ramifications of Equation (2) are extremely important. It is seen that the frequency of torque pulsations, twice slip frequency, decreases as rotor speed increases. Thus, at zero speed, the excitation frequency is equal to two times line frequency or 120 Hz in the United States. As the motor is accelerated, the excitation frequency decreases linearly until it reaches zero when the motor achieves synchronous speed.

The impact that this behavior has on the torsional vibration response of the machine is best illustrated by the Campbell diagram for a hypothetical system presented in Figure 2. In a Campbell diagram, all the unit's torsional natural frequencies are plotted as horizontal lines and the operating (synchronous) speed is denoted by a vertical line. The synchronous motor excitation line is then generated by connecting the point corresponding to twice line frequency (120 Hz) on the y-axis with the point corresponding to synchronous speed (1800 rpm) on the x-axis. Any intersection points between the excitation line and the natural frequency lines (there are three in the figure) are known as interference points. These represent potential resonances that can be triggered during startup.

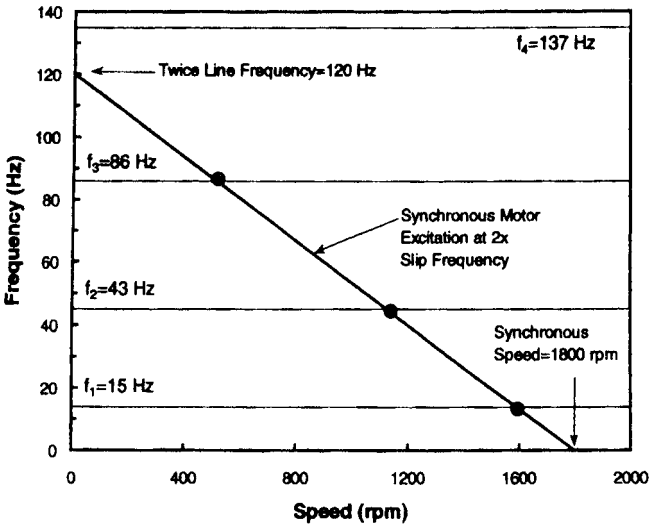

Figure 2. Typical Synchronous Motor Campbell Diagram.

It is easily seen from the figure that the motor generates interferences with all natural frequencies that are below twice line

frequency. This situation is, by no means, unique to the example selected. In fact, all systems driven by synchronous motors will contain interferences with all natural frequencies below twice line frequency that could be excited during starting. This is a significant source of potential problems since most practical turbomachinery drive trains have several natural frequencies within this range.

UNDAMPED ANALYSIS

From the preceding discussion, it is easily seen that all turbomachinery drive trains driven by synchronous motors must be subjected to a rigorous torsional vibration analysis during the design phase of the program to assure structural adequacy. It is, therefore, one of the primary intents of this tutorial to present such a procedure.

Under normal circumstances, the torsional analysis should be performed within 10 weeks of order placement to allow shaft sizes and geometries to be modified without affecting delivery. In addition, it should be provided to each of the individual component vendors to obtain their concurrence. Unfortunately, this analysis is typically among the last analyses to be performed during the design phase so that changes resulting from its performance often impact equipment delivery schedules, sometimes dramatically. The authors cannot overemphasize the perils involved in following this typical path.

The first step in the analysis procedure is the generation of a lumped parameter model such as the simplified one shown in Figure 3. The model consists of a series of interconnected disk and shaft elements. The disks represent the machine's significant inertial components while the shafts behave as torsional springs. Detailed guidelines for generating such a model from hardware drawings are provided in Corbo and Malanoski (1996).

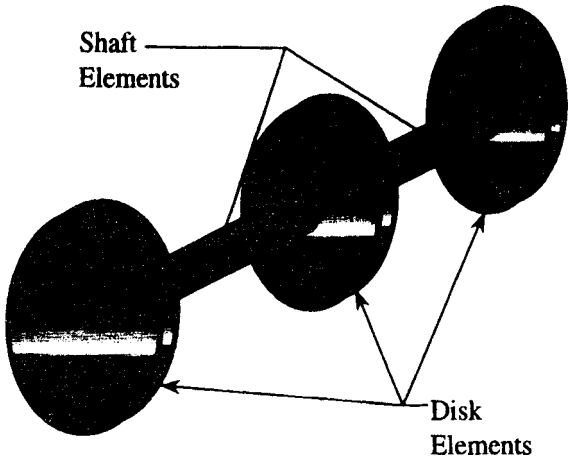

Figure 3. Sample Lumped Parameter Model.

Once the model is completed, the system's undamped natural frequencies should be calculated. Since there is a plethora of computer codes available for performing this computation, no further elaboration is required. Once the computer results are obtained, the authors recommend performing a quick "sanity check" using hand analysis to validate the computer analysis. Several quick methods for doing this are provided in Corbo and Malanoski (1996).

Once the undamped analysis has been validated, a Campbell diagram, similar to that of Figure 2, should be generated. The Campbell diagram allows the determination of the system's potential resonance points and provides an excellent overview of the machine's torsional vibration behavior, analogous to the role played by the critical speed map in a lateral rotordynamics study. For the sake of simplicity, this discussion will focus solely on the excitation generated during the synchronous motor startup. Naturally, in all real systems, there are other excitations present that also must be included in the Campbell diagram.

Once the Campbell diagram has been generated, it should be checked for interference points. In the highly unlikely scenario that there are no such points present, the analysis is finished and the system can be sanctioned. However, the much more probable situation is that there are several such points. In this case, the impact of passing through those resonance points must be evaluated via a transient response analysis of the startup.

TRANSIENT RESPONSE ANALYSIS

In the transient response analysis, the synchronous motor's excitations are applied to the system and the resulting vibratory torques and stresses are computed for each shaft element. Damping due to various sources is included in the model. The induced torques and stresses are then compared to allowable values to determine if the system is structurally adequate.

As was previously stated for undamped natural frequency analysis, there are a number of computer codes available for the transient analysis of torsional systems. The large majority of them use numerical, time-stepping procedures. In these, the differential equations of motion for the lumped model's disks are integrated numerically using methods such as Runge-Kutta and the Newmark-β method. The analysis begins at time zero with all parameters set to their initial values. The numerical approximations, which define a parameter's new value in terms of its previous value, are then used to determine all parameter values after the first time increment. This procedure is continued in a time-marching manner until the machine reaches synchronous speed. This procedure, therefore, estimates the time history of all relevant parameters in the system. Chen (1995), Evans, et al. (1985), and Szenasi and von Nimitz (1978) all discuss numerical integration methods in much greater detail.

In using algorithms employing the Runge-Kutta numerical integration procedure, one with which the authors are intimately familiar, the selection of the time step is critical from the standpoint of solution stability. Per the authors' experience, the time step must be made less than approximately one-fifth the period corresponding to the machine's highest natural frequency. Since a torsional model has as many degrees of freedom (and natural frequencies) as the number of shaft elements in the model, the highest natural frequency for a typical turbomachinery drive train, whose model often contains more than 50 shaft elements, can be astronomically high. Accordingly, if such a model were to be subjected to a time-transient analysis using the Runge-Kutta method, the required time step would be so infinitesimally small that the analysis would be totally impractical.

The authors normally address this problem in one of two manners. The first, and more traditional, method is to reduce the lumped parameter model to a much smaller model, usually consisting of about five disk elements. Since such a model has only four natural frequencies, reasonable time steps can be employed when working with it. Reduction in model size carries a couple of other benefits, as well. First of all, the amount of data generated in the transient analysis of a five-disk model, although still substantial, is much more manageable than that generated when using a much larger model. Secondly, since time-marching analyses require a substantial amount of computer time, the reduction in model size makes the computer time more reasonable. This consideration, a huge one just a few years ago, has lessened in significance with the advent of modern high-speed computers. An example case where an initial model containing 130 stations is reduced to one having only seven is provided by Bogacz, et al. (1990).

The reason that a large multidisk model can be replaced by a much simpler five-disk one without much sacrifice in accuracy is that, in the large majority of practical cases, the only natural frequencies that participate significantly in the synchronous motor startup are the first two (and the second mode's participation is often minor). In fact, Sohre (1965), Pollard (1980), and Wright

(1975) all state that most synchronous motor resonance problems involve only the first (also known as the fundamental) mode. Thus, as long as the simplified model's first two natural frequencies, particularly the first, are reasonably close to those of the original model, the accuracy of the analysis is preserved.

The second method is to employ a transient torsional analysis code that uses modal methods to numerically reduce the system's degrees of freedom. When using such a code, there is no need to reduce the torsional model at all. Since the first (five-disk) method is the more involved and the procedure that was employed in the analysis of the air compressor discussed later, that is the method that will be focused on.

Two basic principles are utilized in the conversion of multidisk models to five-disk ones. The first is that relatively small inertias have very little effect on the machine's first two natural frequencies. These disks can, therefore, be ignored and the shaft elements on either side of them can be combined as springs in series. The second principle is that shafts having relatively large torsional stiffnesses behave as if they were rigid in the first two modes. Accordingly, these elements can be discarded and the inertias on either side of them can be simply added together.

Although some judgment must be exercised in deciding where to place the five disks, some general rules can be stated. The large majority of applications involving synchronous motors that the authors are familiar with involve the motor driving a compressor through a speed-increasing gearbox. In such cases, the authors generally locate one disk at the motor's rotor, one at the gear mesh, and one at the compressor's main wheel. The other two are usually located in the vicinity of the two couplings, one on each side of the gear mesh.

Since some of the transient response programs that the authors have seen do not have the capability of handling multiple shafts rotating at different speeds, it is often necessary to make the five-disk model an "equivalent model" that runs at the motor shaft speed. This model has exactly the same dynamic characteristics and natural frequencies as the actual system. To generate the equivalent model, the parameter values for all elements on the motor shaft are left unchanged. However, all elements on the compressor shaft must be transformed via the following equations:

$$J_{eq} = J \bullet N^2 \tag{3}$$

$$k_{eq} = k \bullet N^2 \tag{4}$$

where:

J_{eq} = Equivalent inertia referenced to motor shaft
J = Actual inertia
N = Gear ratio (ratio of compressor speed to motor speed)
k_{eq} = Equivalent stiffness referenced to motor shaft
k = Actual stiffness

Since the equivalent inertia referred to the motor shaft is equal to the product of the actual inertia and the square of the gear ratio, there is usually a significant difference between the equivalent and actual values. It is, therefore, crucial that the compressor inertia data used for sizing the motor be clearly labeled with regard to the speed that it is relative to.

Once the five-disk model is obtained, an undamped analysis should be run to ensure that its first two natural frequencies have not deviated significantly from those of the original model. If some deviation is observed, the five-disk model should be tweaked to reduce the discrepancies to acceptable levels.

Once the model to be used for the transient analysis is complete, the next step is to specify the machine's performance and damping characteristics. The performance characteristics that are needed include the motor's average and pulsating torques and the compressor's load torque as functions of speed over the entire speed range from standstill to synchronous speed. The need for the pulsating torque is obvious since it represents the excitation being applied to the system. However, the motor's average and compressor's load torques are also important since they determine the machine's acceleration rate.

During startups, the net torque available to accelerate the machine is equal to the motor's average torque minus the load torque. The system acceleration rate in the vicinity of the resonant speed is crucial because it determines the length of time (dwell time) that the machine spends at resonance. The longer the dwell time, the more likely the machine is to experience problems, for two reasons. First, longer dwell times introduce a larger number of damaging high-stress cycles. Second, longer dwell times mean larger torque peaks since they give the response more time to build up toward the steady-state value (which corresponds to an infinite dwell time). Accordingly, designers should aim to maximize the system's acceleration rate in the vicinity of the fundamental mode's resonant speed.

The motor torque should be based on the voltage at the motor terminals, not line voltage. A conservative approach is to not account for any voltage recovery as the train increases in speed. The compressor torque is generally based on throttling the compressor suction to reduce the required horsepower. Care must be taken for refrigeration systems since the compressor suction pressure may settle out at a much higher pressure than under normal operation.

Damping must also be applied to the system in order to limit the response at resonance (which is theoretically infinite for the undamped case) to finite values. The damping due to localized sources can be calculated using the methods given in Corbo and Malanoski (1996) and applied to the appropriate elements. However, the authors have found this to be a time-consuming and often unnecessary step.

Instead, the authors advocate accounting for damping by merely applying a generic damping ratio to each shaft element in the model. This generic ratio accounts for effects, such as hysteretic and slip damping, that are present in all real systems but are extremely difficult to quantify.

A search of the literature revealed some difference in opinion on the magnitude of the damping factor that should be applied. Chen, et al. (1983), cite a typical range of three to five percent of the critical value for geared systems. Anwar and Colsher (1979) are in basic agreement, giving a range of two to five percent. Mruk, et al. (1978), give exactly the same range. Wright (1975) recommends the use of a factor of 1.25 percent for ungeared systems and 2.0 percent for geared machines.

The reason why geared systems are distinguished from ungeared ones is that geared systems generally contain more damping. There are two primary reasons for this. The first is that most turbomachinery gearshafts are supported on fluid-film journal bearings. Although the viscous friction that is inherent in these bearings provides very little damping, if there is any lateral motion accompanying the torsional vibration, the fluid in the bearing's radial clearance is forced to flow circumferentially, thereby generating a squeeze-film effect. Simmons and Smalley (1984), Draminsky (1948), and Shannon (1935) all describe torsional systems in which this was the predominant source of damping in the system. Of course, the torsional-lateral coupling necessary to generate this phenomenon is present only in geared machines.

The second is that, in synchronous motor startups, the cyclic torques occurring at gear meshes at resonance are normally greater than the transmitted torque. In this situation, known as a torque reversal, the resulting negative net torque causes the gear drive surfaces to separate and the teeth to move through their backlash until they make contact on their nondrive surfaces. Once the torque becomes positive again, the teeth are driven back through their backlash until they resume contact on their original surfaces. This results in successive impacts of the gear teeth that dissipate energy via generation of shock waves and eddies. This so-called impactive damping increases the overall system damping.

Thus, the one conclusion that can be drawn from the various references is that the minimum amount of damping that can be expected for a typical geared machine consisting of a motor, gearbox, and compressor is 2 percent of the critical value. Since the authors have found this value to be conservative for such machines, this is the value recommended for use in the absence of actual test data.

Some care should be taken when applying this generic damping ratio since the authors are aware of common misinterpretations that yield incorrect damping coefficients for the individual shaft elements. The damping coefficients for each shaft element, which will all be different, should be calculated using the following:

$$C_n = 2 \bullet \Gamma \bullet k_n / \omega n \tag{5}$$

where:
C_n = Damping coefficient for nth shaft (lbf-sec/in)
Γ = Damping ratio
k_n = Stiffness of nth shaft (lbf/in)
ωn = First torsional natural frequency (rad/sec)

Since torque reversals are commonly encountered, another characteristic of geared machines that is sometimes accounted for in the transient analysis is the backlash between the gear teeth. Including this tends to reduce the predicted peak torques at resonance since the motor's excitation torques are not applied to the compressor shaft during torque reversals. However, Chen, et al. (1983), and the authors have found that the impact of including this effect is usually minor and, thus, recommend conservatively ignoring it.

Once the transient model is completed, the time-transient analysis program should be run to obtain the torque versus time history for each relevant shaft element in the model. A typical plot will look like Figure 4 where the torque cycles at a fairly steady level until resonance with the fundamental natural frequency is approached. At this point, the torque magnitudes begin increasing until they reach a peak at the resonance point. After this, the torque magnitudes begin to decrease until the resonance zone is exited, after which the torques remain fairly constant at a relatively low level.

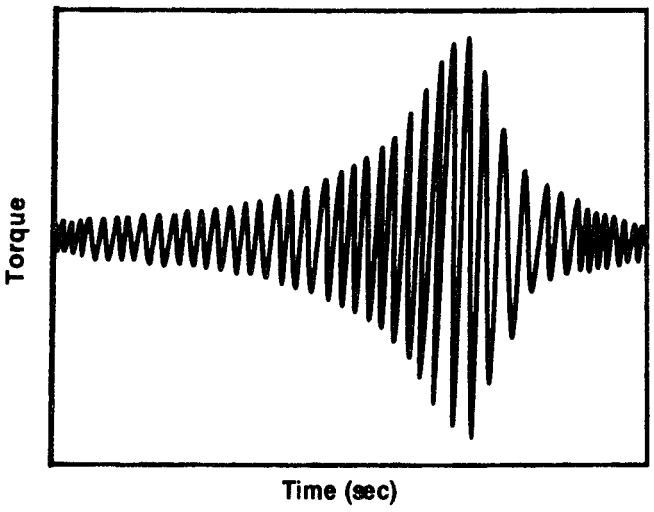

Figure 4. Typical Synchronous Motor Response.

DETERMINATION OF SHAFT FATIGUE LIVES

Once the torque versus time history for a shaft element is known, the life of the shaft can then be calculated. The first step in life determination is the identification of the maximum and minimum torque values for each cycle within the resonance zone. There are a number of ways to convert the results of a transient analysis, which are typically in the form of Figure 4, into a list of cycles having minimum and maximum torques. For the sake of clarity, the descriptions of these methods along with the authors' recommendations will be held off until the example problem is discussed.

The next step is identification of the region or regions within the shaft element that constitute the "weak links" and are most likely to fail. These regions almost always contain geometric stress risers such as steps in shaft diameter and are usually located at relatively small diameters. The one exception to this occurs when the shaft contains a keyway. Since the stress concentration factors arising at keyways are normally very high, regions containing keyways should always be checked out even if they are at large diameters. For the regions of interest, the maximum and minimum torques should be converted to maximum and minimum shear stress values using the following equation from strength of materials:

$$\tau = T \bullet R / I_p \tag{6}$$

where:
τ = Shear stress (psi)
T = Torque (in-lbf)
R = Shaft outside radius (in)
I_p = Shaft area polar moment of inertia (in^4)

The maximum and minimum shear stresses so obtained should then be combined to obtain the cyclic stress occurring in each torque cycle. It should be noted that in fatigue problems such as this where the mean stress is nonzero, it is technically necessary to calculate both the mean and cyclic stresses in order to determine life. However, Evans, et al. (1985), Walker, et al. (1981), and the authors have found that in synchronous motor startups, the magnitude of the mean stress is so much lower than that of the cyclic stress that the mean stress can be safely ignored. Thus, only the cyclic stress needs to be calculated, using the following equation:

$$\tau_{cyclic} = 0.5 \bullet \left(\tau_{\max} - \tau_{\min}\right) \tag{7}$$

where:
τ_{max} = Maximum stress
τ_{min} = Minimum stress
τ_{cyclic} = Cyclic stress

Determination of the cyclic stress is the easy part of the life prediction procedure. The part that confuses many engineers is the determination of the allowable stress that this cyclic stress should be compared to. Although the authors do not pretend that the procedure that follows is the only legitimate one that can be used for this, they do believe that it is more accurate than the large majority of methods currently being used.

Strain-Life Theory of Failure

The primary difference between the advocated procedure and most other procedures currently being used is that it relies on the strain-life theory of failure rather than the traditional S-N curve (stress-life theory). When the traditional S-N curve is employed, it is implicitly assumed that the life of a part is directly dependent on the level of stress it carries. On the other hand, the strain-life theory is based on the empirical finding that the parameter that determines the life of a part is strain (i.e., displacement), not stress (i.e., load).

In the traditional stress-life method, stress is plotted versus number of cycles on log-log paper. Shigley and Mischke (1989) speak for many authors when they advocate the following simple method for generating the S-N curve. In the absence of more precise test data, the tensile endurance limit can be approximated as being equal to one-half the material's ultimate tensile strength and should be taken to correspond to a life of 10^6 cycles. In the low cycle fatigue (LCF) regime, the strength at a life of 10^3 cycles should be set equal to 90 percent of the ultimate tensile strength. The complete S-N curve can then be generated by connecting these two points by a straight line on a log-log plot of stress versus life.

Shigley and Mischke (1989) point out that the S-N curve generated via the above procedure has the following governing equations:

$$S(N) = a \bullet N^b \tag{8}$$

$$a = (.90 \bullet UTS)^2 / Se \tag{9}$$

$$b = -1/3 \bullet \log(.90 \bullet UTS / Se) \tag{10}$$

where:
N = Number of fully-reversing cycles
S(N) = Cyclic stress corresponding to a life of N cycles (psi)
UTS = Ultimate tensile strength (psi)
Se = Tensile endurance limit (psi)
a, b = Empirical constants

The use of the S-N curve is quite simple. For a given fully-reversing stress level, the above equations or the plot can be used to find the life corresponding to that stress.

Although the traditional stress-life method is a perfectly acceptable procedure for evaluating the fatigue lives of shafts, it tends to be conservative due to the following two effects:

- Most experts agree that the endurance limit corresponds to a life somewhere between 10^6 and 10^7 cycles. Accordingly, assuming that the life corresponding to the endurance limit strength is only 10^6 cycles is conservative.

- Shigley and Mischke (1989) state that in order for a fatigue failure to occur, cyclic plastic deformations must be present. Boyer (1986) concurs, stating that fatigue failures are the product of the simultaneous action of cyclic stresses, tensile stress, and plastic strain. Since the presence of plastic strain is needed for a fatigue failure to occur, the life of a part is a function of both its strength and its ductility. Since the stress-life method does not account for ductility effects, it tends to underpredict the lives of parts made from ductile materials.

The strain-life theory deviates from this by assuming that the life of a part is dependent on the level of strain, not stress, occurring in the part. Shigley and Mischke (1989) speak for most experts in the field when they claim that the strain-life theory is the best existing theory for predicting fatigue failures. This is consistent with the authors' experience that the stress-life method, while being perfectly valid, tends to be conservative. On the other hand, the strain-life theory, while still erring on the conservative side, is a much more accurate predictor of shaft life.

The basis of the strain-life theory is that the relationship between applied strain and life is as illustrated in Figure 5, taken from Shigley and Mischke (1989). It is seen from the figure that the total strain in a part is the sum of the elastic strain and the plastic strain. It is also seen that both the elastic and plastic strains are linearly related to part life when plotted on log-log paper. For this reason, this theory is also commonly referred to as the universal slopes theory. It is further seen that, in the high cycle fatigue (HCF) regime, the total strain is primarily elastic strain. On the other hand, in the low cycle fatigue region, the plastic strain predominates.

Boyer (1986) points out that most people arbitrarily set the dividing line between low and high cycle fatigue somewhere between 10^4 and 10^5 cycles. However, a more accurate dividing criterion is whether the predominant component of strain imposed during cyclic loading is elastic or plastic. In fact, Mischke (1982) defines the dividing line between LCF and HCF as the point where the elastic and plastic strains are equal.

The baseline equation for the strain-life theory is the Coffin-Manson equation, which assumes that the total strain versus life curve behaves in the manner of Figure 5:

$$\varepsilon(N) = (\sigma_f` / E) \bullet N^b + \varepsilon_f` \bullet N^c \tag{11}$$

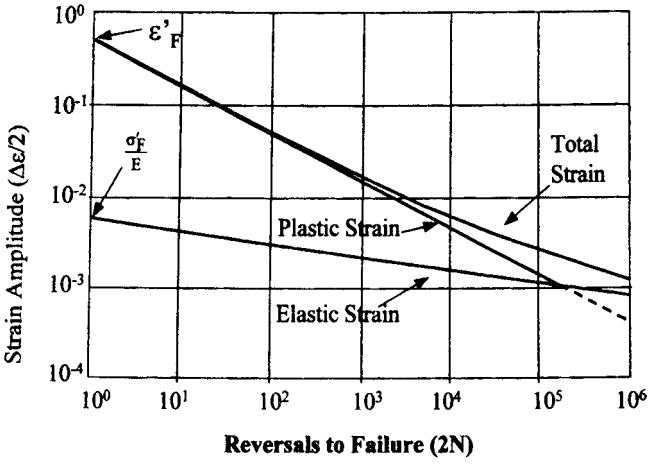

Figure 5. Typical Strain Versus Life Curve.

where:
N = Life (cycles)
ε(N) = True strain corresponding to a life of N cycles
$\sigma_f`$ = True stress at fracture during tensile test (psi)
$\varepsilon_f`$ = True strain at fracture during tensile test
b = Elastic strain exponent (slope of elastic strain line)
c = Plastic strain exponent (slope of plastic strain line)
E = Elastic modulus (psi)

Equation (11) is the equation that the authors advocate using for determining the strain versus life behavior of a given shaft subjected to torsional vibration. The elastic and plastic strain exponents are material characteristics that can be obtained from Boyer (1986), Shigley and Mischke (1989), or any other resource containing material fatigue properties. The true stress and true strain at failure can be directly obtained from the tensile test results per the following:

$$\sigma_f` = UTS / (1 - RA) \tag{12}$$

$$\varepsilon_f` = ln(1 / (1 - RA)) \tag{13}$$

where:
UTS = Ultimate tensile strength (psi)
RA = Reduction in area

It is seen that whereas the stress-life method did not take the material's ductility into account, the strain-life method accounts for the material's reduction in area, a direct measure of ductility.

Equation (11) gives the strain versus life characteristics for any shaft element of interest. However, unless a finite element code is employed during the transient startup analysis, the strains imposed on the shafts are usually unknown. Instead, the known parameter for each shaft element is stress. The logical question is then how the relation of Equation (11) can be converted into an equation, similar to Equation (8), relating stress and life.

In an attempt to answer this question, the authors consulted with a number of fatigue experts of their acquaintance. The consensus of these experts was that the strain-life curve should be converted into a stress-life curve by merely multiplying the strains by the material's elastic modulus, *E*. This is not purely correct since the assumption that the stress is equal to the product of the strain and the elastic modulus is only valid for elastic strains. As is shown by Mischke (1982), the relationship between plastic stresses and strains is much more complex.

However, the experts justified their recommendation by noting that for the large majority of synchronous motor startup calculations, the portion of the curve that is of interest is the portion where the elastic strain is greater than the plastic strain. This is because the proposed version of API 617 indicates that compressors being

driven by synchronous motors are generally capable of surviving at least 1500 starts. Thus, using Miner's cumulative damage rule, which will be described in detail later, with a limiting summation value of 0.5 and assuming 10 torsional cycles per start, the smallest number of allowable cycles will be 30,000 (1500 • 10 / 0.5). In fact, in the example provided later to illustrate the authors' procedure, the smallest number of allowable cycles is 61,600, which lies in the HCF region of the strain versus life curve for most engineering materials. Accordingly, the error introduced by making an approximate conversion of plastic strain to stress is small.

In order to test the validity of this recommendation, the authors used the recommended procedure on a 4340 steel shaft and compared its results with those obtained using the much more complicated procedure given by Mischke (1982). As expected, the allowable stress at a life of 1000 cycles predicted by the recommended procedure was about three times that predicted by the more sophisticated method. However, at a life of 10,000 cycles, the recommended procedure overpredicts the strength by about 35 percent and, at a life of 30,000 cycles, it is only 7.5 percent high. At lives above 40,000 cycles, there is virtually no difference between the two methods. Accordingly, it is concluded that merely multiplying the strains of Equation (11) by the elastic modulus to obtain stresses is perfectly valid for the large majority of synchronous motor startup problems that the user is likely to encounter. However, the user should always remember the limitations of this method when dealing with small numbers of cycles.

Strength Derating Factors

Multiplication of Equation (11) by the elastic modulus yields the baseline tensile stress versus life curve for the shaft material of interest. This curve must then be multiplied by a number of factors to obtain the shear stress versus life curve for the actual shaft element, as follows:

$$\tau(N) = S(N) \bullet Fsh \bullet ka \bullet kb / (kf \bullet SF) \tag{14}$$

where:
τ(N) = Allowable shear stress for a life of N cycles (psi)
N = Number of fully-reversing cycles
S(N) = Allowable tensile stress for a life of N cycles (psi)
Fsh = Shear factor
ka = Surface finish factor
kb = Size factor
kf = Fatigue stress concentration factor
SF = Safety factor

In the authors' experience, determination of the derating factors in Equation (14) is one of the most confusing and misunderstood aspects of analyzing synchronous motor startups. For that reason, the proper method for determining each of these factors will be discussed in detail.

Shear Factor

The shear factor, *Fsh*, is included to reflect that a material's strength in shear is less than its tensile strength. This factor is merely the ratio of a material's shear strength to its tensile strength for the same number of applied cycles. There are two major failure theories, both discussed in Shigley and Mischke (1989), for determining this factor. The more conservative theory is the maximum shear stress theory, which predicts that this ratio is 0.50. The second theory is the distortion energy (AKA von Mises) theory, which gives this ratio as 0.577.

The authors are acquainted with some engineers, such as Szenasi and von Nimitz (1978), who believe that the maximum shear stress theory should be used for synchronous motor startups because it is more conservative. However, it is the authors' experience that the distortion energy theory is a more accurate predictor of the actual shaft strength. This viewpoint is shared by Banantine, et al. (1990), Juvinall (1967), and Shigley and Mischke (1989). Accordingly, the authors advocate the use of the distortion energy theory and a shear factor of 0.577.

Surface Finish Factor

The surface finish factor, *ka*, accounts for the fact that the susceptibility of a part to fatigue failures can be drastically reduced by improving its surface finish. This is because the scratches, pits, and machining marks that are more prevalent in a rough surface add stress concentrations to the ones already present due to part geometry. Since most published material properties are obtained from tests performed on finely polished specimens, the fatigue strengths of most parts will be less than the published values. The surface finish factor represents the ratio of the part's fatigue strength to that of the test specimen, based on surface finish considerations.

Shigley and Mischke (1989) provide the following equation for calculating the surface finish factor:

$$ka = a \bullet UTS^{b} \tag{15}$$

where:
ka = Surface finish factor
UTS = Ultimate tensile strength (ksi)
a, b = Empirical coefficients dependent on manufacturing method

Coefficients *a* and *b* are given in Table 7-4 of Shigley and Mischke (1989) for various surface finishing processes. For machined surfaces, *a* is equal to 2.70 and *b* equals −0.265. Although it is not explicitly listed in the table, the surface finish factor for a polished surface is 1.0.

Most of the engineers of the authors' acquaintance account for surface finish effects by utilizing the above factor to derate the strength at all lives on the S-N curve. The authors feel that this is overconservative since Boyer (1986) points out that the surface finish factor calculated using the above equation only applies to the endurance limit at 10^6 cycles. At all other lives, the effect of surface finish is reduced until a life of 1000 cycles is reached, where it has no effect whatsoever (ka = 1.0).

Although Boyer (1986) does not give any methodology for determining the surface finish factor at lives between 1000 and 10^6 cycles, using the same arguments that are provided later for the size and stress concentration factors, the authors have assumed that the relationship between surface finish factor and life is linear when plotted on log-log coordinates. Utilizing that assumption, the relevant equations for surface finish factor as a function of life can be shown to be as follows:

$$ka(N) = 10^{b} / N^{m} \tag{16}$$

$$m = \log\left[ka(1000) / ka(10^6)\right] / 3.0 \tag{17}$$

$$b = \log\left\{\left[ka(1000)\right]^2 / ka(10^6)\right\} \tag{18}$$

where:
ka(N) = Surface finish factor for a life of N cycles
$ka(10^6)$ = Surface finish factor for 10^6 cycles (from Equation (15))
ka(1000) = Surface finish factor for 1000 cycles (1.00)
m = Slope of ka versus N line on log-log coordinates
b = Intercept of ka versus N line on log-log coordinates

Thus, it is seen that the surface finish factor varies from a maximum value of 1.0 at 1000 cycles to a minimum value of that given by Equation (15) at 10^6 cycles.

Size Factor

The size factor accounts for the empirical observation that when two shafts are manufactured from the same batch of material and

tested at the same level of surface strain, the larger diameter shaft will almost always fail in a lower number of cycles than the other shaft. There are three general theories for why this size effect exists. The first recognizes that fatigue failures almost always initiate at the location of a flaw in the material. Since a shaft containing a larger volume of material is statistically more likely to contain such a flaw, the susceptibility of a shaft to fatigue failure increases with shaft diameter.

The second theory is very similar to the first except that it is based on surface area instead of volume. This theory states that since almost all fatigue failures initiate at a flaw on the surface of a part, larger parts are more vulnerable since they have larger surface areas and are, thereby, more likely to contain surface flaws.

The third theory, as espoused by Banantine, et al. (1990), is based on the assumption that the susceptibility of a part to fatigue failure is directly dependent on the volume of the thin layer of surface material that is subjected to a stress level within 95 percent of the stress at the surface. Since a larger component will have a shallower stress gradient than a smaller part, the larger part will have a larger volume subjected to this high stress. This makes the larger part more vulnerable to fatigue failures. Empirical results that reveal that size effects are much less important for axial loadings, where there is no stress gradient, than for bending or torsional loadings provide backing for this hypothesis.

Regardless of what mechanism is at work, there is no question that larger shafts subjected to torsional loadings will fail in less cycles than smaller shafts. Additionally, since most shafts used in practical turbomachines are larger than the 0.25 to 0.30 inch diameter shafts usually used to generate published strength data, the size effect almost always involves a reduction in strength. This is accounted for via the size factor, *kb*, which is defined as the ratio of the strength of the part to the strength of the test specimen.

In a search of the literature, the authors found a number of empirical relations for size factor. A number of these are summarized in Table 13-3 of Shigley and Mischke (1986). One that is not tabulated is given by Shigley and Mischke (1989) as follows:

$$kb = \left(d \,/\, 0.3\right)^{-0.1133} \tag{19}$$

where:
kb = Size factor
d = Shaft diameter (in)

Another relation that the authors have found to be useful is given by Banantine, et al. (1990):

$$kb = 0.869 \bullet d^{-0.097} \tag{20}$$

where:
kb = Size factor
d = Shaft diameter (in)

Regardless of which method is used to determine it, the authors have found that, similar to the surface finish factor, many engineers erroneously believe that the size factor should be applied to the entire S-N curve. This is refuted by Banantine, et al. (1990), who state that the size effect is observed mainly in the HCF regime. Juvinall (1967) agrees, stating that the effect of part size on static strength and strength at 1000 cycles is much less pronounced than at 10^6 cycles and is commonly neglected.

Accordingly, using the same reasoning as was used for the surface finish factor, the authors advocate using the size factor obtained from the above empirical relations only with the strength for 10^6 cycles. At a life of 1000 cycles, a size factor of unity should be employed, and at all lives between these two points, the size factor versus life characteristic should be assumed to follow a linear relation when plotted on log-log coordinates. The relevant equations are very similar to those previously given for the surface finish factor:

$$kb(N) = 10^{b} \,/\, N^{m} \tag{21}$$

$$m = \log\left[kb(1000) \,/\, kb\left(10^6\right)\right] / 3.0 \tag{22}$$

$$b = \log\left\{\left[kb(1000)\right]^2 \,/\, kb\left(10^6\right)\right\} \tag{23}$$

where:
kb(N) = Size factor for a life of N cycles
kb(10^6) = Size factor for 106 cycles (from Equation (19) or (20))
kb(1000) = Size factor for 1000 cycles (1.00)
m = Slope of kb versus N line on log-log coordinates
b = Intercept of kb versus N line on log-log coordinates

Stress Concentration Factor

The fatigue stress concentration factor, *kf*, is included in Equation (14) since, in the authors' experience and that of Jackson and Umans (1980), almost all torsional vibration fatigue failures occur at locations of geometric stress concentrations such as fillet radii or keyways.

The fatigue stress concentration factor, *kf*, is arrived at by first determining the geometric stress concentration factor, *kt*. This factor is solely dependent on the geometry of the stress raiser and is totally independent of the part's material and condition. Peterson (1974) gives geometric stress concentration factors for virtually any geometry that the user is likely to encounter. Finite element analysis is another effective method for determining values of *kt*.

The geometric stress concentration factor is determined assuming that the part is made from an ideal material that is isotropic, elastic, and homogeneous. Fortunately, the deviations from these assumptions that occur in real materials tend to reduce the impact of the stress raiser. To account for these real effects, a second stress concentration factor, *kf*, which is always less than or equal to *kt*, is defined as follows:

$$kf = 1 + q\left(kt - 1\right) \tag{24}$$

where:
kf = Effective stress concentration factor
kt = Geometric stress concentration factor
q = Material notch sensitivity

It is seen that the geometric and effective stress concentration factors are related by a parameter, *q*, that represents how sensitive the material is to notches. The notch sensitivity factor is defined by the above equation and, by definition, is always between zero and one. A material having a notch sensitivity of zero is totally insensitive to notches such that its effective stress concentration factor is always 1.0, regardless of notch geometry. On the other hand, a material having a notch sensitivity of one is extremely sensitive to the presence of notches and, as a result, its geometric and effective stress concentration factors are equal.

In general, the notch sensitivity factor is dependent on the material, its heat treatment, and the size of the notch in question. Juvinall (1967) and Shigley and Mischke (1989) both give plots that can be used to determine the notch sensitivity factor for most practical cases. Once the notch sensitivity is obtained, it should be combined with the geometric stress concentration factor using Equation (24) to obtain the effective stress concentration factor, *kf*.

As was the case with the surface finish and size factors, the effective stress concentration factor determined in the above manner only applies at a life of 10^6 cycles. However, unlike the surface finish and size factors, there is some disagreement over how much the impact of stress concentrations is reduced at a life of 1000 cycles. Shigley and Mischke (1989) recommend that, similar to the cases for surface finish and size factors, the life of 1000 cycles be treated as a static loading case that has a corresponding *kf* value of 1.0. Evans, et al. (1985), are more conservative, recom-

mending that the square root of the *kf* value corresponding to 10^6 cycles be used at 1000 cycles.

To resolve this discrepancy, the authors turned to Juvinall (1967) who acknowledges that many experts have assumed that the effects of stress raisers are negligible at lives up to 1000 cycles. However, he goes on to say that recent experiments have clearly indicated that this assumption is overly optimistic. Accordingly, the authors have adopted the method of Evans, et al. (1985), by using the following equation:

$$kf(1000) = \left[kf\left(10^6\right)\right]^{0.5} \tag{25}$$

where:
kf(1000) = Effective stress concentration factor for 1000 cycles
kf(10^6) = Effective stress concentration factor for 10^6 cycles

Once the two endpoints are known, there is nearly unanimous agreement on how *kf* values between 1000 and 10^6 cycles should be determined. Shigley and Mischke (1989), Evans, et al. (1985), and Juvinall (1967) all agree that the *kf* versus *N* characteristic is linear when plotted on log-log coordinates. The reasoning behind this is that doing so keeps the S-N curve linear on log-log coordinates, which agrees with empirical findings. It is this reasoning that was used previously for deciding that the surface finish and size factors should also exhibit the same behavior as a function of life. Parroting the equations previously provided for the surface finish and size factors, the equations for determining *kf* are as follows:

$$kf(N) = 10^b \,/\, N^m \tag{26}$$

$$m = \log\left[kf(1000) \,/\, kf\left(10^6\right)\right] / 3.0 \tag{27}$$

$$b = \log\left\{\left[kf(1000)\right]^2 \,/\, kf\left(10^6\right)\right\} \tag{28}$$

where:
kf(N) = Effective stress concentration factor for a life of N cycles
kf(10^6) = Effective stress concentration factor for 10^6 cycles (from Equation (24))
kf(1000) = Effective stress concentration factor for 1000 cycles (from Equation (25))
m = Slope of kf versus N line on log-log coordinates
b = Intercept of kf versus N line on log-log coordinates

It should be noted that the procedure provided herein utilizes the stress concentration factor as a strength reduction factor (per Equation (14)) rather than in the more conventional role of a stress increasing factor. If *kf* were independent of life, the two methods would be equivalent and could be used interchangeably. However, since *kf* is a function of life, it must be used as a strength reduction factor. Thus, the user should remember to not apply a stress concentration factor to the cyclic stress obtained from Equation (7) since stress concentration effects are already accounted for in the S-N curve.

Safety Factor

In a previous paper (Corbo and Malanoski (1996)), the authors reported that an extensive literature search revealed a near unanimous consensus that a safety factor of 2.0 should be employed when comparing calculated and allowable stresses for torsional vibration analyses. However, these recommendations were almost all concerning the safety factor to be applied to the results of a steady-state torsional response analysis. In the authors' experience, the primary reasons why a safety factor is needed for torsional analyses are the inherent uncertainties in the magnitudes of the excitation torques and in the generic damping ratio that is normally applied to each shaft element in the system. However, as Smalley (1983) has noted, the results of a transient response analysis, such as the one under consideration, are much less sensitive to errors in the damping coefficient than are the results of a steady-state response analysis. Furthermore, the magnitudes of the excitation torques in steady-state analyses are usually more uncertain since they are usually based on rules of thumb, whereas synchronous motor startup analyses use the actual motor excitation torques. Based on this, the authors have reasoned that a safety factor somewhat lower than the steady-state value of 2.0 would be appropriate for a synchronous motor startup analysis.

Accordingly, the authors sought to determine what transient analysis safety factor would be equivalent to the universally accepted steady-state safety factor of 2.0. In order to do this, the authors made a series of transient and steady-state response runs on a representative synchronous motor-driven compressor. For all runs, all parameters were held constant except for the damping ratio, which was systematically varied. Thus, the difference in excitation uncertainties was conservatively ignored and the function of the safety factor was assumed to be solely to account for damping coefficient uncertainties.

The results of these runs are plotted in Figure 6. The abscissa for this plot is the assumed damping ratio while the ordinate is the ratio of the maximum calculated cyclic torque to that obtained using the baseline damping ratio of 2.0 percent. It is easily seen that, as expected, the steady-state runs are far more sensitive to variations in the assumed damping ratio than are the transient runs. Furthermore, it is seen that a 2:1 variation in damping ratio results in a 2:1 change in steady-state response since the response is merely inversely proportional to the damping ratio. However, a 2:1 change in damping ratio results in only about a 30 percent change in the peak torque of the transient analysis. Conservatively assuming that the conventional steady-state safety factor of 2.0 is used to accommodate a 2:1 uncertainty in damping, it is seen that this same uncertainty can be accommodated with a safety factor of about 1.3 for the transient case. For the sake of conservatism, the authors recommend using a safety factor of 1.35 for transient analyses.

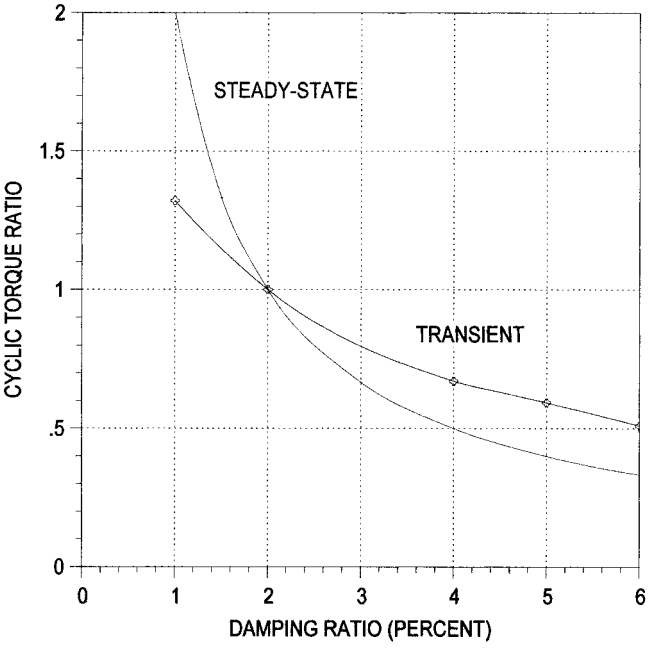

Figure 6. Effects of Varying Damping Ratio.

Once all the derating factors have been determined, the allowable shear stress versus number of cycles curve can be obtained from Equation (14). For each life of interest, Equations (16), (21), and (26) should be used to calculate the surface finish,

size, and effective stress concentration factors. These should then be combined with the S-N curve obtained by multiplying Equation (11) by the elastic modulus, the shear factor of 0.577, and the safety factor of 1.35 to determine the allowable shear stress for that life. A series of these calculations can then be used to generate the τ-N curve.

Cumulative Damage Determination

The preceding text provides a method for determining the allowable number of cycles for a given torsional cyclic stress level calculated via Equation (7). If each startup consisted of a single stress cycle repeated a given number of times, the machine's allowable number of starts could be easily determined. However, since the cyclic torque versus time profile typically looks like that of Figure 4, a shaft element will normally be subjected to a number of different cyclic stress levels during a single startup.

Consequently, the shaft's life must be predicted using some type of cumulative damage algorithm. Accordingly, the authors recommend employment of Miner's linear damage rule, which is described in detail by Miner (1945) and is probably the simplest cumulative damage algorithm in common usage. The basis of Miner's rule is that each individual stress cycle where the stress is above the endurance limit consumes a fraction of the part's total life. The fraction of life lost is given by the following:

$$f_I = n_I / N_i \tag{29}$$

where:
f_I = Fraction of life lost
n_I = Total number of applied cycles of given cyclic stress
N_I = Allowable number of cycles for given cyclic stress

For example, if a shaft is subjected to 1500 starts and each start has one loading cycle having a cyclic stress of 25,000 psi, the number of applied cycles would be 1500. Furthermore, if the τ-N curve generated for this shaft using the procedure previously described revealed that the number of allowable cycles for a stress level of 25,000 psi was 15,000 cycles, then *N* would be 15,000. The fraction of the part's life consumed by this loading cycle would then be 10 percent (1500/15,000).

Theoretically, the part should fail when the summation of the individual life fractions obtained from the above equation equals unity. However, many experimenters have found that the sum at which parts actually fail can vary somewhat from this value. Juvinall (1967) tells of tests in which the summation at failure varied from 0.61 to 2.20. Shigley and Mischke (1989) disagree slightly, claiming that the observed range is from 0.70 to 2.20. Based on these findings and their own experience, the authors have adopted a value of 0.50 as a safe limit for synchronous motor startups. Thus, a part is assumed to fail when:

$$\Sigma \left(n_I / N_I \right) = 0.50 \tag{30}$$

Using this rule, the number of starts that a shaft can be safely subjected to can be directly calculated. First, the allowable number of cycles, N_I, for each cyclic stress above the endurance limit that the shaft is subjected to should be determined from the τ-N curve. Then for an assumed number of starts, the number of applied cycles for each cyclic stress, n_I, should be calculated. The fractional damages can then be calculated from Equation (29) and the sum of the fractions can be compared to 0.50. The number of starts that gives a sum of exactly 0.50 is the allowable number of starts.

The authors are fully confident in the use of this procedure even though they are fully aware that some experts such as Manson, et al. (1965), correctly criticize Miner's rule for its failure to account for the order that the stresses are applied in. It is well known that if a part is subjected to its peak stress cycle first and then subjected to progressively decreasing stress cycles, it will fail much quicker than if the stresses are applied in a random order. Under these circumstances, use of Miner's rule will overpredict the part's life. Juvinall (1967) asserts that parts have been observed to fail at a summation of as low as 0.18 when the stresses were applied in this manner.

On the other hand, if the stress cycles are sequentially increased with the peak stress cycle being the last one applied, the life of a part can be dramatically increased. In fact, many investigators have observed that this phenomenon, known as coaxing, results in an increase in the material's endurance limit above its virgin value. For these conditions, Miner's rule underpredicts life, sometimes dramatically. Juvinall (1967) has observed parts that have lasted all the way up to a sum of 23.0 when loaded in this manner.

Fortunately, in synchronous motor startups, the loading is not even close to either of these two extremes. It is the authors' experience that in most synchronous motor startups, the peak stress cycle is chronologically near the middle of the high-stress cycle range such that the number of high-stress cycles occurring before it is about equal to the number after it. This is illustrated in Figure 4. Thus, for this case, the shortcomings of Miner's method are felt to be inconsequential. This conclusion is backed up by Evans, et al. (1985), Wachel and Szenasi (1993), Anwar and Colsher (1979), Joyce, et al. (1978), and Jackson and Umans (1980), all of whom recommend using Miner's rule in the evaluation of synchronous motor startups.

The number of stress cycles that must be included in the Miner's summation varies with the application. As a rule of thumb, Sohre (1965) states that a typical startup involves from 10 to 20 high-stress cycles. The exact number of cycles that have to be considered in the Miner's summation is determined by converting the minimum and maximum torque values into cyclic stresses via Equations (6) and (7). These cyclic stresses should then be compared to the shear endurance limit obtained from Equation (14) since the only cycles that contribute to fatigue damage are those where the cyclic stress exceeds the endurance limit. All such cycles need to be included in the Miner's summation. All other cycles can be discarded.

OTHER STRUCTURAL CONSIDERATIONS

In addition to the ability of the shafts to withstand the required number of starts, several other structural issues must be looked at when evaluating the results of a synchronous motor startup analysis. The peak torques occurring in specialty components such as gears, splines, and couplings should be compared to the component's maximum torque rating to prevent overloading. The peak torques occurring at interference fits retaining wheels, gears, or coupling hubs should also be checked to verify that they are not large enough to cause relative motion to occur.

In stark contrast to the steady-state situation, torque reversals occurring at components, such as gears, splines, or couplings, that contain backlash are not a concern in the transient case. Under normal circumstances, these components are continuously loaded in one direction and the system operates totally unaware of the backlash. However, if the magnitude of the induced vibratory torque exceeds the average transmitted torque, the net torque becomes instantaneously negative and a torque reversal is said to have occurred. Whereas this condition can be disastrous in the steady-state, Szenasi and von Nimitz (1978) and Grgic, et al. (1992), note that transient torque reversals are quite common and are normally allowed for in the design of gears and geared couplings.

MODIFICATIONS TO ALLEVIATE PROBLEMS

If the results of the startup analysis meet all the structural criteria given above, the analysis is finished and the machine can be sanctioned. However, in the event that the original design is found wanting, some methods of rectification are as follows:

• *Alter the starting procedure to start the compressor in the unloaded condition*—If the motor must start the compressor in the loaded condition, the compressor load torque is usually quite high. Accordingly, the system's acceleration rate is relatively slow and the dwell time at resonance is, thereby, relatively long. Starting the compressor in the partially or fully unloaded condition will normally speed up the acceleration significantly and reduce the dwell time at resonance. This results in a reduction in peak torque due to insufficient time for it to build up to its previous value as well as a reduction in the number of damaging cycles per startup.

• *Reduce the inertia of the load*—Many authors have noted that synchronous motor startups are more likely to generate problems as the ratio of the load inertia to that of the motor increases. This is probably due to an increased dwell time at resonance, similar to the situation described above.

• *Reduce the motor voltage during starting*—Since the magnitudes of the motor's pulsating torques are approximately proportional to the square of motor voltage, this can result in a significant reduction in the system's peak torques and stresses. The downside of doing this is that it also reduces the motor's average torque, causing the startup to take longer and increasing the dwell time at resonance. However, in the authors' experience, the benefits usually outweigh the drawbacks and many practical machines are started at between 70 and 90 percent of full voltage.

• *Change the motor shaft's coupling to a special damping coupling*—The authors are familiar with many synchronous motor-driven turbomachines that are equipped with a Holset-style coupling on the motor shaft. These couplings contain an elastomeric element that tends to damp out (via material hysteresis) the pulsations generated in the motor. Additionally, placement of this coupling on the motor shaft tends to isolate the excitation source (motor) from the areas where trouble is frequently encountered (gearbox and compressor).

• *Make changes to increase the fundamental frequency*—As was stated previously, most synchronous motor startup problems involve resonance with the fundamental frequency. It is the experience of the authors, and many other experts, that the lower this natural frequency is, the more likely the machine will encounter problems. The explanation for this is twofold. First, as is seen from Figure 2, the lower the fundamental frequency is, the higher its resonant speed will be. Since most motors' pulsating torques increase significantly as synchronous speed is approached, high resonant speeds usually mean large excitations. Second, synchronous motor average torques tend to decrease near synchronous speed such that the machine's acceleration rate tends to be relatively slow as synchronism is approached. Accordingly, resonance dwell times are increased. Thus, any changes that can be made (usually implemented at the motor coupling) to increase the fundamental frequency are usually beneficial.

• *Polish or shotpeen any troublesome shafts*—The beneficial effects that employing a finer surface finish have on fatigue life have already been discussed. However, shotpeening critical shaft surfaces can also result in significantly increased fatigue strengths, sometimes by as much as 30 to 40 percent. The reason for this improvement is that shotpeening leaves the surface in a state of residual compression. Since fatigue failures can only occur if tensile stresses are present, the residual compression must be overcome before the surface stress can become tensile.

• *Alter the motor design so that the crossover point occurs close to resonance*—As is depicted in Figure 1, many synchronous motors have a point somewhere in their speed range where the direct and quadrature axis torques are equal (crossover point). Since the pulsating torque is equal to the difference in these two torques, it is zero at this point. Accordingly, if the motor design can be altered such that the crossover point occurs in the vicinity of resonance, the potential for problems is greatly reduced.

• *Alter the motor and/or system to increase the acceleration at resonance*—Since both the motor's average torque and the compressor's load torque are highly nonlinear as a function of speed, the net torque available to accelerate the machine tends to vary as a function of speed. The net acceleration torque can, thus, be plotted as a function of speed and changes enacted to locate the problem resonant point at a point where the acceleration torque is high to minimize the dwell time at resonance.

• *Change the motor from a solid pole to a laminated rotor design*—In general, laminated rotors tend to generate lower pulsating torques than do solid pole designs and, thus, are less likely to generate problems. However, implementing this change can introduce other problems. Since laminated pole synchronous motors often have average torque versus speed curves that contain large positive slopes, a negative damping effect that can trigger instability problems can result. Additionally, laminated pole motors tend to be more expensive.

If any modifications are implemented, a new system has been created. Accordingly, the entire torsional analysis procedure must be repeated to verify that the change has not introduced any new problems.

OVERALL ANALYSIS PROCEDURE

All the steps of the analysis procedure have been described in detail. To recap, a chronological listing of the steps to be taken is as follows:

1. Generate lumped parameter model.
2. Determine undamped natural frequencies and mode shapes.
3. Verify undamped analysis results using hand calculations.
4. Generate Campbell diagrams.
5. Reduce lumped parameter model in preparation for transient analysis (if necessary).
6. Verify that first two natural frequencies of reduced model are same as for original model.
7. Run synchronous motor startup analysis.
   - Input motor average and pulsating torques and load torques as functions of speed.
   - Select appropriate damping ratio to apply to all shafts in model.
   - Select time step to avoid numerical instabilities.
   - Obtain torque versus time histories for all shaft elements.
8. Select shaft elements to run fatigue calculations on
   - Shafts having small diameters.
   - Shafts having significant stress concentrations.
   - Any shaft containing a keyway.
9. For each shaft of interest, determine the strain-life curve from Equation (11).
10. Generate the baseline tensile stress versus life curve by multiplying the strain-life curve by the elastic modulus.
11. Determine the geometric stress concentration factor, kt, from the shaft's geometry.
12. Determine the notch sensitivity factor, q.
13. Determine the effective stress concentration factor, kf, for 10^6 cycles from Equation (24).
14. Determine the surface finish factor, ka, for 10^6 cycles.
15. Determine the size factor, kb, for 10^6 cycles.
16. Using Equations (16), (21), and (26), calculate kf, ka, and kb as functions of life, N.
17. Using a shear factor of 0.577, a safety factor of 1.35, and Equation (14), determine τ-N curve.
18. Using Equations (6) and (7), calculate cyclic shear stress, t_{cyclic}, for each high-stress cycle.
19. Use τ-N curve to find allowable number of cycles, N, for each value of cyclic shear stress.

20. Determine number of starts that makes Equation (30) true. This is the allowable number of starts.
21. Check for any other structural problems.
22. If necessary, implement modifications to alleviate structural problems.
23. Repeat above procedure for new system resulting from step 22 changes.

EXAMPLE ILLUSTRATING ANALYTICAL PROCEDURE

The presented procedure is best illustrated by an example. The authors recently completed the design of a 66,000 hp air compression unit. The centrifugal compressor, which runs at 4298 rpm, is driven by a synchronous motor operating at 1800 rpm through a one-stage stepup gearbox. Both the high- and low-speed shafts contain flexible diaphragm couplings.

Per the advocated procedure, a lumped parameter model was constructed for the entire drive train and undamped analysis was run on it. The first two natural frequencies, whose mode shapes are presented in Figures 7 and 8, were found to occur at 14.0 and 34.0 Hz. A Campbell diagram (not shown) was then generated to account for the system's steady-state excitations and no steady-state resonance points were found. The motor shaft Campbell diagram of Figure 9 was then generated to determine the potential resonances triggered by the synchronous motor excitation.

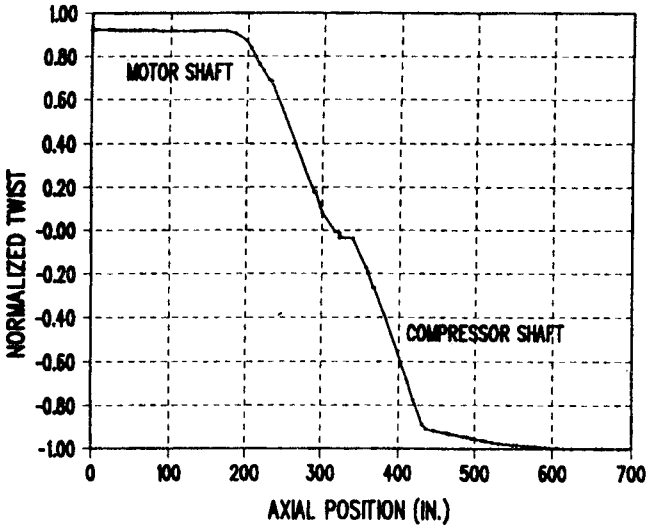

Figure 7. Air Compressor First Mode Shape.

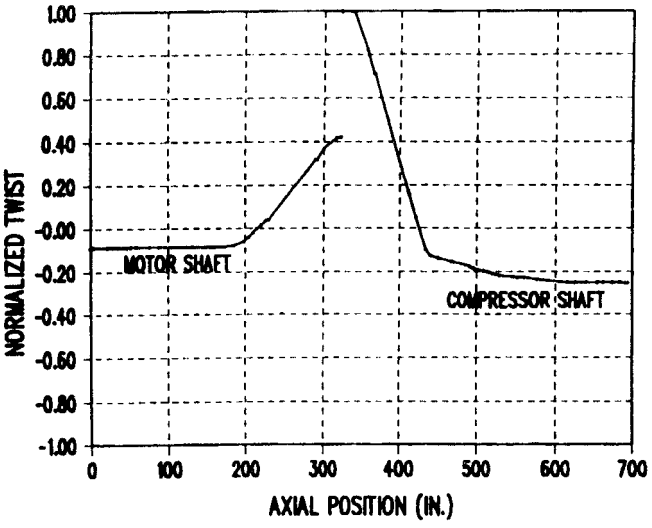

Figure 8. Air Compressor Second Mode Shape.

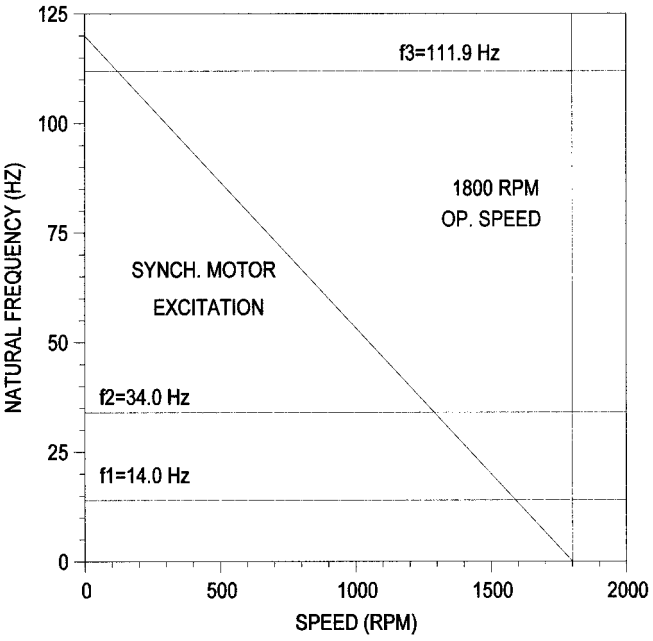

Figure 9. Air Compressor Campbell Diagram.

It is seen from the figure that the synchronous motor excitations create three resonance points—with the first, second, and third natural frequencies. Per the authors' experience, the resonance with the third natural frequency was ignored since that frequency seldom participates in synchronous motor responses, especially when its resonance point is at such a low speed. Thus, the transient response analysis focused on simulating the responses at the first two natural frequencies with the fundamental being the primary concern since its resonance point occurs at such a high speed (1590 rpm or 88 percent of synchronous speed).

To accommodate the limitations of the transient response analysis program employed, the original model, which contained 74 stations, was reduced to an equivalent five-disk model. Each shaft element in the model represented one of the primary shafts in the drive train—motor shaft, gearshaft, pinion shaft, and compressor shaft. Undamped analysis was then performed on the reduced model and the first two natural frequencies were verified to still be at 14.0 and 34.0 Hz.

Once the reduced model was validated, the transient analysis was run. Since the undamped analysis revealed that the reduced model's highest (fourth) natural frequency occurred at 115.3 Hz, its corresponding period was 0.0087 seconds. In accordance with the guidelines provided previously, a generic damping ratio of 2 percent of the critical value and a time step of 0.001 seconds were employed. Gear backlash effects were ignored.

The results of the transient analysis consisted of the time histories of the torque in all four shafts. These plots revealed that the response as the system passed through the resonance with the second mode was inconsequential. However, as expected, a significant resonance was observed at a motor speed of about 1608 rpm, representing excitation of the fundamental frequency at 14.0 Hz.

The response in the resonance region for the motor shaft is presented in Figure 10. It should be noted that the torque plotted as the ordinate is expressed in the peculiar units of "per unit" (pu). This is a shorthand method of expressing the ratio of the actual torque to the motor's rated torque at synchronous speed. For this motor, one pu is equal to 2.31E6 in-lb.

Examination of the figure reveals that the torque is fairly smooth up until resonance is approached. In this region, the mean torque is seen to be positive, representing the torque required to drive the load. The relatively small ripple that is superimposed on the mean torque represents the relatively small response to the synchronous motor's pulsations.

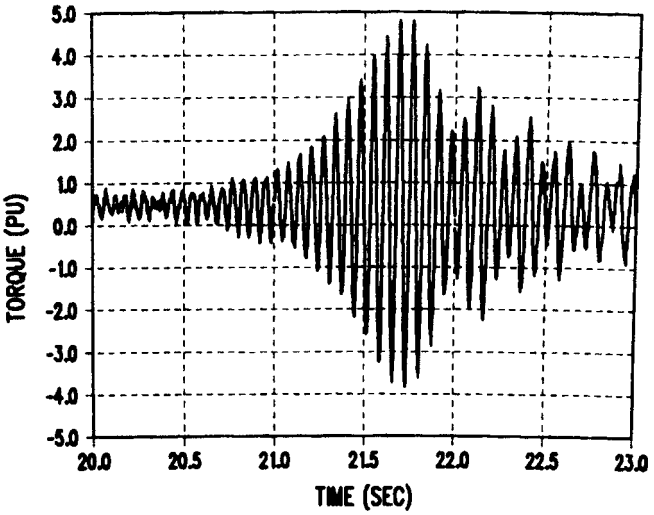

Figure 10. Air Compressor Calculated Response.

Once the resonance zone is entered at about 21.2 seconds, the ripple rises steadily until it reaches a peak at about 21.75 seconds. At this peak, the maximum torque is seen to be almost 5.0 pu while the minimum is almost −4.0 pu. Referral to the speed versus time plot (not shown) revealed the speed at this peak to be about 1608 rpm, confirming that the unit is in resonance with its first natural frequency. The peak torque is followed by several more high torque cycles of progressively smaller amplitudes until the torque once again levels off as the resonance zone is exited.

Although all four shafts had similar response profiles and were analyzed to determine how many starts they could take, this discussion will only consider the motor shaft. The first decision that needed to be made was which portion of the shaft represented the "weak link." Although this decision is not always straightforward, in this case it was since the shaft's smallest diameter also contained a significant stress concentration. The shaft diameter at that location was 13.17 inches.

Attention then turned to generating the allowable shear stress versus number of cycles curve for this shaft. The shaft material was 4340 stainless steel, which had an ultimate strength of 120,000 psi and a reduction in area of 40 percent. Accordingly, using Equations (12) and (13), the Coffin-Manson coefficients were calculated to be 200,000 psi ($\sigma_f`$) and 0.5108 ($\varepsilon_f`$). Using these values with empirically-determined proprietary values for the exponents, *b* and *c*, in Equation (11), the strain-life curve was generated. Multiplying all strain values by the elastic modulus of 28.5 million psi then yielded the tensile stress versus life curve for the polished test specimen.

Using the plot for a filleted shaft under torsional loading found in Peterson (1974), the geometric stress concentration factor, *kt*, was estimated to be 1.55. Using Juvinall (1967), the notch sensitivity, *q*, was then determined to be 0.91. Substituting these values into Equation (24), the effective stress concentration factor, *kf*, for a life of 10^6 cycles was found to be 1.501.

Using Equation (15), the 10^6 cycle surface finish factor was calculated to be 0.90 for the ground surface.

Determination of the size factor was not as simple as merely using Equation (19) or (20) since the shaft's diameter was so large that it was outside the size range that the providers of those relations claimed they were valid for. Accordingly, proprietary test data was utilized to come up with a size factor of 0.667 for a life of 10^6 cycles. It should be noted that the predictions of Equations (19) and (20), 0.651 and 0.677, respectively, are close enough to the empirically derived value that the authors feel that either of those equations can probably be used in this size range.

Once the values of *ka*, *kb*, and *kf* were obtained for a life of 10^6 cycles, the values at all other lives were determined. Using the equations provided previously, the slopes (*m*) and intercepts (*b*) for these three parameters on log-log coordinates were determined to be:

- Surface finish factor: m = 0.015252, b = 0.045757
- Size factor: m = 0.058625, b = 0.175874
- Stress concentration factor: m = 0.029373, b = 0.0

Using these values in Equations (16), (21), and (26), the variations of the three factors with life were calculated and are presented in Table 1. Then, employing these factors, a shear factor of 0.577 and a safety factor of 1.35, the baseline tensile S-N curve was converted to a τ-N curve using Equation (14). Selected values from this curve are also tabulated in Table 1.

Table 1. Air Compressor Allowable Stresses.

ALLOWABLE CYCLES N	K_A	K_B	K_F	ALLOWABLE SHEAR STRESS (PSI)
1000	1.000	1.000	1.225	119,302
2000	0.989	0.960	1.250	83,495
3000	0.983	0.938	1.265	68,725
5000	0.976	0.910	1.284	54,612
7500	0.970	0.889	1.300	46,066
1.0E4	0.965	0.874	1.311	41,092
1.5E4	0.960	0.853	1.326	35,288
2.0E4	0.955	0.839	1.338	31,864
2.5E4	0.952	0.828	1.346	29,534
3.0E4	0.949	0.819	1.354	27,813
4.0E4	0.945	0.806	1.365	25,386
5.0E4	0.942	0.795	1.374	23,716
6.0E4	0.939	0.787	1.381	22,470
7.0E4	0.937	0.780	1.388	21,492
8.0E4	0.935	0.773	1.393	20,696
9.0E4	0.934	0.768	1.398	20,029
1.0E5	0.932	0.763	1.402	19,460
1.5E5	0.926	0.745	1.419	17,479
2.0E5	0.922	0.733	1.431	16,248
3.0E5	0.917	0.716	1.448	14,715
5.0E5	0.910	0.695	1.470	13,059
7.5E5	0.904	0.678	1.488	11,922
1.0E6	0.900	0.667	1.501	11,194

Once the τ-N curve was obtained, the next task was to determine the number of applied stress cycles for each start and the stress levels corresponding to each cycle. There are a number of ways to convert the results of a transient analysis in the form of Figure 10 to a tabulation of stress cycles having minimum and maximum stresses. Jackson and Umans (1980) discuss the peak counting method in which each cycle is merely assumed to have a cyclic torque that is equal to the peak torque obtained from the transient analysis. For instance, the peak torque occurring in Figure 10 is +4.811 pu. Thus, using the peak counting method, the cycle would be assumed to consist of a torque range from −4.811 to +4.811 pu. This is obviously overconservative since the minimum torques displayed in Figure 10 all have magnitudes below 4.0 pu and are not recommended for use.

Jackson and Umans (1980) then proceed to describe a less conservative cycle counting procedure known as the rainflow method. Although this method is probably the most accurate one available for analyzing profiles where the torque varies randomly, the authors do not believe that its complexity is warranted for the predictable profiles obtained from synchronous motor startups. Instead, the authors have had considerable success using a simple chronological counting procedure. The peak torque is identified and the minimum torques preceding and succeeding the peak

torque are then checked. Whichever minimum torque has the greater magnitude is paired with the peak torque and all other torque peaks are then paired in the same manner.

Use of this procedure is illustrated by referral to Figure 10. As stated previously, the peak torque is +4.811 pu. The minimum torque peaks preceding and following this peak are −3.743 and −3.848 pu, respectively. Since the following peak has a larger magnitude, it is selected for pairing with the +4.811 pu peak. Accordingly, the first torque cycle is assumed to be from +4.811 to −3.848 pu. All other cycles are determined by pairing the positive peak with the negative peak immediately following it. The resulting torque cycles obtained from applying this procedure to the profile of Figure 10 are presented in Table 2.

Table 2. Air Compressor Cumulative Damage Assessment.

PEAK NO.	DESCRIPTION	T_{MAX} (PU)	T_{MIN} (PU)	T_{MAX} (IN-LBF)	T_{MIN} (IN-LBF)	τ_{MAX} (PSI)	τ_{MIN} (PSI)	τ_{CYCLIC} (PSI)	APPLIED CYCLES n	ALLOW CYCLES N	n/N
1	PEAK	4.811	-3.848	1.11134E7	-8.88888E6	24,778	-19,818	22,298	7307	61,608	0.119
2	PEAK + 1	4.802	-3.615	1.10926E7	-8.35065E6	24,731	-18,618	21,675	7307	67,963	0.108
3	PEAK + 2	4.236	-2.867	9.78516E6	-6.62277E6	21,816	-14,766	18,291	7307	125,945	0.058
4	PEAK + 3	3.170	-1.641	7.32270E6	-3.79071E6	16,326	-8,451	12,389	7307	628,026	0.012
5	PEAK - 1	4.434	-3.743	1.02425E7	-8.64633E6	22,836	-19,277	21,057	7307	75,235	0.097
6	PEAK - 2	3.974	-3.249	9.17994E6	-7.50519E6	20,467	-16,733	18,600	7307	118,225	0.062
7	PEAK - 3	3.415	-2.589	7.88865E6	-5.98059E6	17,588	-13,334	15,461	7307	244,197	0.030
8	PEAK - 4	2.959	-2.176	6.83529E6	-5.02656E6	15,239	-11,207	13,223	7307	474,108	0.015

Once the method for determining torque cycles had been decided on, the next order of business was determining how many cycles needed to be considered. In order to determine this, the torque values were converted into cyclic stress values via Equations (6) and (7). These cyclic stresses were then compared to the shear endurance limit, which is seen to be 11,194 psi from Table 1. Thus, all cycles having a calculated cyclic stress of 11,194 psi or greater were retained and the remaining ones were discarded. It is seen from Table 2 that doing this eliminated all but eight stress cycles. In addition to the peak cycle, there are the four cycles immediately preceding it (denoted in the table by N-1, N-2, etc.) and the three cycles immediately following it.

For each of these cycles, the cyclic stress is used with the τ-N curve to determine the allowable number of cycles, *N*. For instance, for the peak cycle, which has a cyclic stress of 22,298 psi, referral to Table 1 reveals that *N* is somewhere between 6.0E4 and 7.0E4 cycles. Using the actual equation, *N* is computed to be 61,608 (6.16E4) cycles. The allowable number of cycles for all other stress cycles was calculated in exactly the same manner.

The only remaining task is the calculation of the allowable number of starts for this shaft. For this case, which is highly typical of synchronous motor startups, each stress cycle is applied only once per startup. Thus, if the unit were subjected to *n* startups, the applied number of cycles for each tabulated cycle would be *n*. Although *n* can still be determined by trial and error, rearrangement of Equation (30) yields the following explicit relation for *n*:

$$n = 0.5 / \Sigma \left(1 / N_I\right) \tag{31}$$

where:

n = Allowable number of starts

N_I = Allowable number of cycles for Ith cycle

Using this equation, the allowable number of starts is calculated to be 7307. When this value is substituted for n in Table 2, it is verified that the sum of the expended lives is approximately 0.50, in accordance with Miner's rule. Since this unit was required to demonstrate structural integrity for 5000 starts, this shaft was declared fully satisfactory.

ADVANTAGES OF NEW PROCEDURE OVER TRADITIONAL METHOD

The reader may not yet grasp the significance of the advantages that utilizing the shaft life prediction rules provided herein have over the traditional method. After all, many of the rules, such as assuming that the surface finish factor is variable instead of constant, may appear to merely be small tweaks to the conventional method. However, the log-log nature of the τ-N curve means that small changes in predicted strength translate into large changes in predicted life. This large gain can be appreciated by examination of Table 1. It is seen that the strength for 10^4 cycles is 41,092 psi while that for 10^5 cycles is 19,460 psi. It is, thereby, seen that a 2:1 change in strength corresponds to a 10:1 change in life. Accordingly, use of each of the rules presented herein yields a significant increase in predicted life compared to the conventional method.

To illustrate how powerful these effects are, the authors have run a number of cases for the motor shaft described in the previous example and the results are presented in Table 3. Case A is the one presented in the example using the new procedure. All other cases were run by changing one of the new procedure's rules back to its counterpart in the traditional method. The impact of the rules changes advocated herein can, thereby, be clearly seen.

Table 3. Impact of Varying Model Assumptions.

CASE	DESCRIPTION	ALLOWABLE NUMBER OF STARTS	PERCENT CHANGE FROM BASELINE
A	BASELINE - RECOMMENDED PROCEDURE USED	7307	-
B	STRESS LIFE THEORY USED INSTEAD OF STRAIN-LIFE THEORY	2237	-69.4 %
C	K_F ASSUMED CONSTANT AT 10^6 CYCLES VALUE	5562	-23.9 %
D	K_A ASSUMED CONSTANT AT 10^6 CYCLES VALUE	6382	-12.7 %
E	K_B ASSUMED CONSTANT AT 10^6 CYCLES VALUE	4011	-45.1 %
F	MAX SHEAR STRESS THEORY USED INSTEAD OF VON MISES	4346	-40.5 %
G	SAFETY FACTOR CHANGED TO 2.0	1940	-73.5 %
H	ALL ABOVE CHANGES APPLIED TOGETHER	56	-99.2 %

In case B, the strain-life procedure for determining the τ-N curve was replaced by the traditional stress-life method described previously. It is seen that this change alone results in a reduction in predicted life from 7307 to 2237 starts, a huge reduction. This is consistent with the advantages of using the strain-life theory cited by other authors.

In cases C, D, and E, the traditional method of applying the 10^6 cycle values of *kf*, *ka*, and *kb* to the entire S-N curve is employed. It is seen that all these changes have significant impact, especially that involving the size factor, *kb*. This large effect is due to the large diameter shaft being studied and should not be as dramatic for more conventional shaft sizes.

In case F, the method of calculating the shear strength from the known tensile strengths has been changed from the maximum shear stress theory to the distortion energy (von Mises) theory. Although the two theories do not appear to differ that much (.500 versus .577 factor), the impact of the change is seen to be substantial.

In case G, the stress safety factor has been changed from the recommended value of 1.35 to the traditional value of 2.00. The change in predicted life is amazingly high, suggesting that the large majority of organizations performing torsional analyses are over-conservative.

Finally, in case H, all the traditional rules are used together. It is seen that doing this reduces the predicted number of starts from 7307 to a mere 56. Thus, the traditional method predicts that a perfectly good shaft has virtually no startup capability whatsoever. The authors hope that the advantages of using the new procedure are now making themselves apparent to the reader.

FUNDAMENTALS OF STRAIN GAUGE TESTING

The use of strain gauge sensors for mechanical testing is a mature, and often misunderstood, technology. Perhaps it is the straightforwardness of the underlying principles on which these types of measurements are made that make it confusing to engineers? In most cases, the extremely small geometric changes that occur when a mechanical component is exposed to load cannot be detected via visual inspection. For example, a typical mechanical component, such as a link of steel chain, may only stretch 0.000025 to 0.00010 inches under normal operating load. For the past 50 or so years, engineers have been reliably measuring these types of small displacements using fundamental electrical circuits. The most common approach to measuring small displacements is to adhere a length of conductive media to the mechanical component being tested (e.g., a link of steel chain) and monitor the media's change in electrical resistance as the component is being loaded—a strain gauge. What facilitates much of the misunderstanding concerning usefulness of this technology is that, more often than not, the only exposure to strain gauges many engineers receive is in a laboratory environment, where these gauges are commonly used as a vehicle to measure the strain in tensile test specimens. Accordingly, many engineers develop the misconception that strain gauges can only be used to measure the performance of basic mechanical components (e.g., a tensile specimen) under simple, static loads. To the contrary, over the years, numerous industrial sensor technologies have been developed using strain gauges as the basis for their measurements—load cells and accelerometers, to name a couple.

One of the primary objectives of this tutorial is to acquaint engineers who are unfamiliar with the practical implementation of strain gauge technologies with an overview of how strain gauges can be used to accurately measure the transmitted dynamic torque in mechanical drive trains. It is not the intention of this tutorial to train and/or instruct engineers concerning the installation/setup of strain gauge sensors. Rather, the purpose here is to educate engineers/managers who may be considering the use of strain gauges to measure the torsional performance of drives on the basic electromechanical principles of this technology, as well as the quality and quantity of data they can expect to obtain.

The opening portion of this section of the tutorial is intended to be a general primer on torsional strain gauge measurements for rotating systems. How are the measurements made? What kind of equipment is required? Once understood, the technological "risks" are discussed and several common "Do's and Don'ts" of strain gauge testing are presented.

The measurement of dynamic torque via strain gauges is a viable technique that can be readily used to validate analytically based performance predictions (e.g., the dynamic torques occurring during the startup of a synchronous drive). With proper installation techniques and good data acquisition/measurement practices, torque measurement accuracies within 5 percent can be expected. The following section discusses some of the basic concepts of the strain gauge sensor, electrical circuits, and associated signal conditioning/telemetry hardware to provide an understanding of the types of issues that are associated with torsional shaft measurements.

As shown in Figure 11, the active element of a strain gauge is its measurement grid. The gauge vendor calibrates the grid, a precisely engineered pattern of deposited conductive alloy, so that the engineer can relate its change in resistance as a function of its stretch. The gauge's calibration factor, commonly referred to as the "gauge factor," relates the ratio of the change in its electrical resistance to the measured strain according to the following equation:

$$GF = \left(\Delta R / R_{nom}\right) / \left(\Delta L / L\right) \tag{32}$$

where:

ΔR = Change in grid resistance (ohms)
R_{nom} = Nominal grid resistance (ohms)
ΔL = Change in grid length (inches)
L = Nominal grid length or "gauge length" (inches)

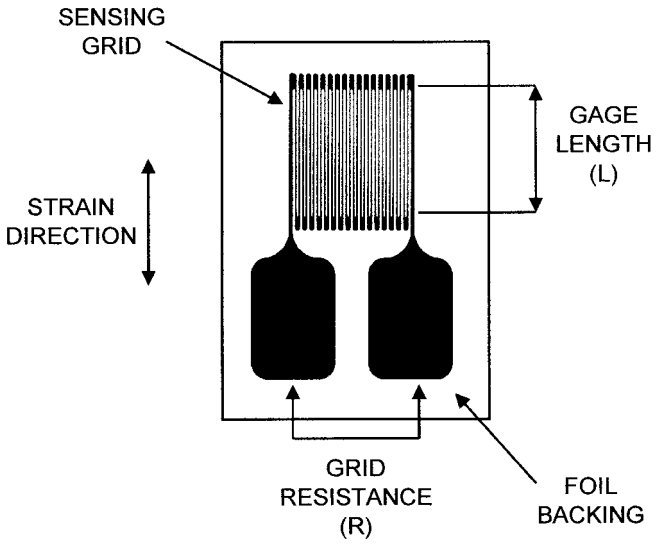

Figure 11. Strain Gauge Basic Elements.

As tension is applied to a strain gauge, its electrical resistance increases due to two effects. The first is that the tensile elongation increases the effective length of the gauge. The second is that the Poisson effect causes the conductor to neck down, reducing its cross-sectional area. Since resistance is directly proportional to length and inversely proportional to cross-sectional area, both these phenomena yield increased resistance.

Typical of most electrical resistance strain gauges, the active grid is bonded to a foil substrate. This arrangement of grid/substrate is commonly referred to as a foil gauge. Foil gauges are attached to the measurement surface via a thin layer of high performance adhesive. Suitable adhesives for this application usually have fast curing times (requires a curing agent), and exhibit high strength/low creep qualities. Accordingly, recognizing that mechanical strain is transferred to the gauge via the glue line, it is obvious that the integrity of the adhesive bond is critical to the performance of the gauge. Typical values for the nominal gauge factor and grid resistance of most modern foil strain gauges are 2.0 and 350 ohms, respectively.

At this point it is appropriate to utilize a practical example to provide an "order of magnitude" estimate of the sensed quantity (change in electrical resistance) that is typical of most strain gauge work. For the sake of this example, consider an application where a single strain gauge is adhered to a mechanical component subjected to pure bending. The mechanical strain at the outer fibers of the component where the gauge is mounted is 500 ˘ 10 6 inches/inch (microinches). Rearranging the equation for the gauge factor (Equation 32) and utilizing the aforementioned gauge factor and resistance values, the anticipated change in electrical resistance can be computed according to the following relationship:

$$\text{Resistance change} = (\text{mechanical strain}) \times (\text{gauge factor}) \times (\text{gauge resistance})$$
$$\Delta R = 500 \times 10^{-6} \times 2.0 \times 350$$
$$\Delta R = 0.175 \text{ ohms}$$

For those who are unfamiliar with the measurement of electrical quantities, the reliable measurement of a change in resistance of 0.175 ohms out of a nominal resistance of 350 ohms (a change of 0.05 percent) would be difficult to make with an ohmmeter. Fortunately, there are alternative ways of measuring this behavior.

To facilitate the requisite measurement of small changes in resistance, strain gauges are typically electrically configured in

what is commonly know as a Wheatstone Bridge circuit. In lieu of providing a comprehensive presentation of the mathematics behind the Wheatstone Bridge circuit, the salient point of understanding to take away from this tutorial is that the bridge circuit permits the indirect measurement of small changes in electrical resistance via a "readily made" measurement of differential voltage (typically on the order of a few millivolts).

A graphical representation of the Wheatstone bridge, herein referred to as the bridge circuit, is presented in Figure 12. As is shown in this figure, a bridge circuit containing a single active leg (one containing a strain gauge) is commonly known as a "quarter bridge." It is seen that the other three legs simply contain fixed resistors. Figure 13 illustrates how a single quarter bridge circuit might be configured to measure mechanical strains associated with beam bending. Referring to the arrangement diagramed in Figures 14 and 15, the use of four strain gauge sensors in a common bridge circuit (a "full bridge") can result in as much as a fourfold increase in the sensitivity of measured differential voltage across the bridge for the same strain field. There are also other advantages to using a full bridge configuration that will become apparent later on in this tutorial. Although, it is beyond the scope of this tutorial, interested readers can find the derivations of the governing equations for the behavior/performance of the bridge circuit in almost all basic textbooks covering electrical theory.

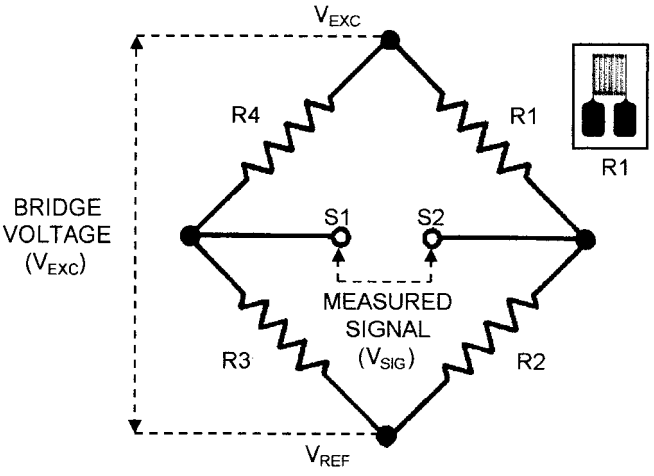

Figure 12. Wheatstone Bridge—Quarter Bridge Circuit.

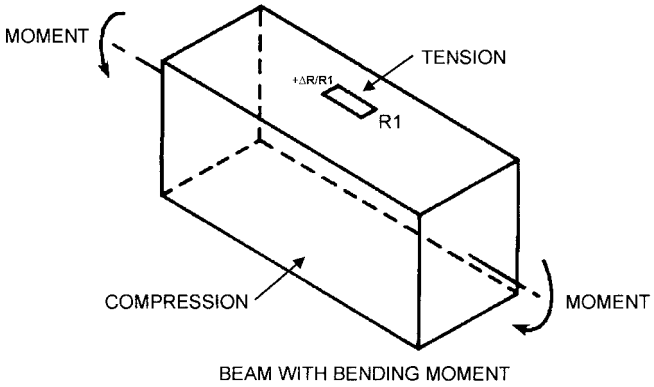

Figure 13. Measurement of Bending Strains with a Single Gauge.

Up to this point, the basic operation of the strain gauge has been discussed without regard to the application of torsional shaft measurements. Now the aforementioned basics of strain gauge theory will be combined with the elastic strain-displacement theory for a circular shaft segment exposed to a torsional moment to illustrate how strain gauges can be configured to measure dynamic shaft torque.

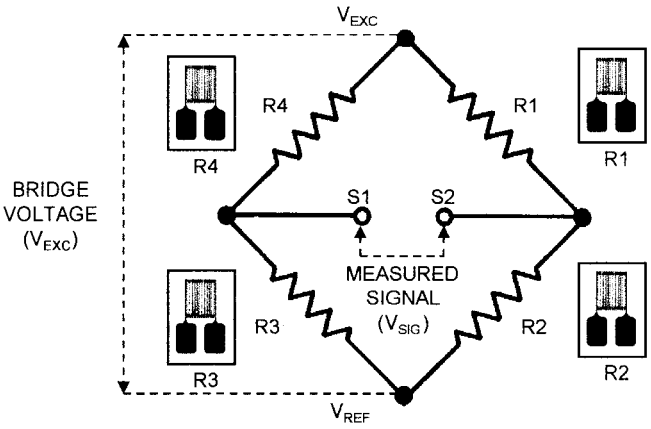

Figure 14. Wheatstone Bridge—Full Bridge Circuit.

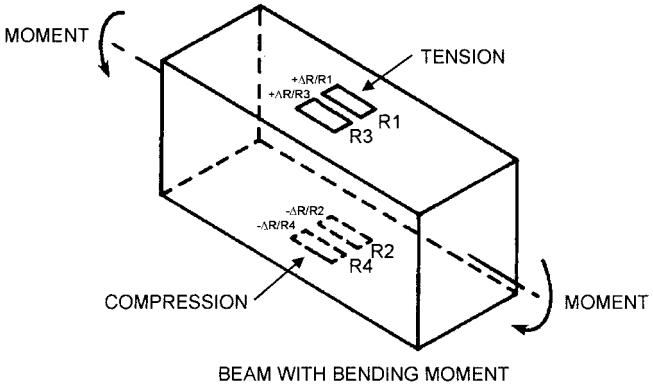

Figure 15. Measurement of Bending Strains with Four Strain Gauges.

As is illustrated in Figure 16, per the basic principles of elasticity, a circular shaft section under the influence of a torsional moment develops maximum and minimum principal shearing strains that are oriented at ±45 degree angles with respect to the torsional twist axis. Further, owing to the symmetry of the shaft geometry, as well as the applied torsional loading, the two principal strains (tension and compression) are equal in magnitude. Accordingly, it is apparent that orienting the strain gauge grid on the shaft in a direction corresponding to either of the two 45 degree principal strains will optimize the sensing of mechanical strain. In fact, as is shown in Figure 17, going one step further and utilizing four separate strain gauge grids that are oriented along the ±45 degree principal strain directions and configuring them in a full bridge circuit will increase the sensitivity of the measured differential voltage across the bridge (proportional to the shaft torque) by a factor of four! Recognizing the utility of this gauge configuration, most vendors offer a variety of two-element 90 degree torque rosettes (two sensing grids at ±45 degrees on a common foil backing) for torque measurement applications. The design of the gauge's sensing grid is highly optimized to measure torsional strains and minimize influence of unwanted transverse strains. Referring again to Figure 17, note that a further refinement to the full bridge strain gauge layout is made by locating each 90 degree rosette at diametrically opposite locations on the shaft. Using this gauge configuration, the unwanted influence of bending and/or shearing strains resulting from shaft flexure is electrically cancelled by the bridge circuit.

Most field measurements of torsion are made at an interior location along the drive train (typically between the prime mover and the driven component), thereby requiring that the transmission of the strain gauge bridge signal be made from the rotating shaft to a stationary receiver via telemetry. Fortunately, as a consequence

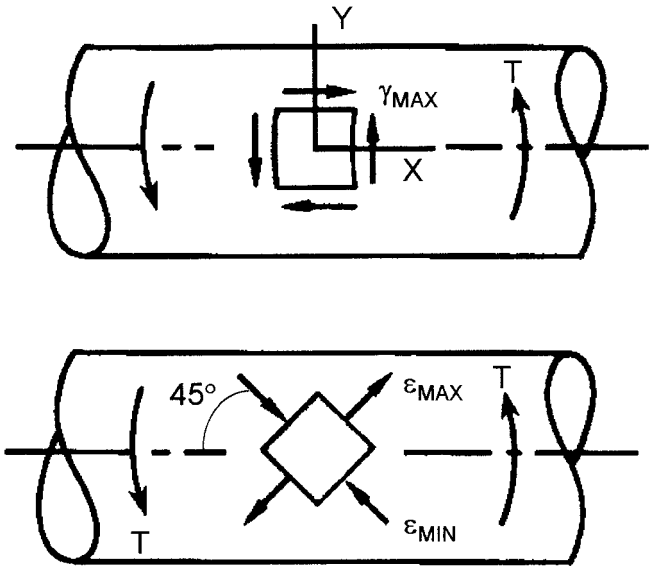

Figure 16. Circular Shaft Section with Torsional Moment.

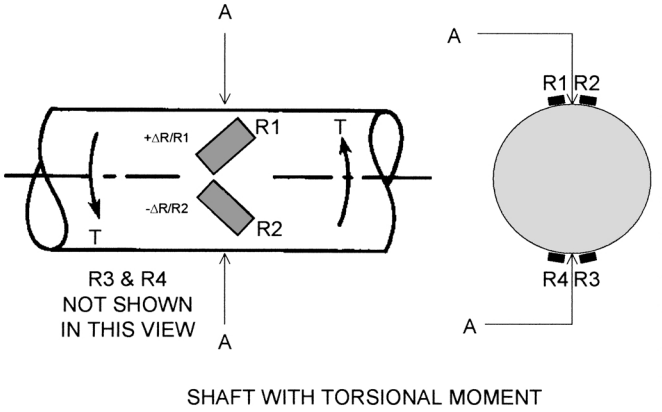

Figure 17. Circular Shaft Section with Four Strain Gauges.

of the rapid progression of semiconductor technologies over the last decade, there are a number of compact digital telemetry systems to choose from.

As part of the transmitter's design, most telemetry systems provide an onboard regulated power supply for the bridge circuit, as well as a programmable gain amplifier to increase the differential bridge voltage signal to levels that can be accurately recorded by most data acquisition hardware (typically ±10 volts). In addition, many good digital telemetry systems, which operate at transmission frequencies in the 900 MHz range, permit the transmitter/receiver to operate at different carrier frequencies within the 900 MHz band to avoid local radio interference. The transmitting hardware of just about all the telemetry systems can provide several hours of uninterrupted service when powered by a single nine volt alkaline battery.

To compute a theoretical sensitivity for the torsional strain gauge application, the engineer must have accurate data for the shaft geometry/material, strain gauge calibration, and the telemetry settings/configuration. Similar to an accelerometer or proximity probe sensor, the computed sensitivity for the torsional strain gauge measurement establishes the relationship between the telemetry output signal voltage and the mechanical shaft torques. In the context of most computer-based data acquisition systems, the sensitivity value is the numerical input that permits the system to display the acquired data in terms of the desired engineering units (in-lbf, ft-lbf, etc.). For most of these systems, the sensitivity is defined as millivolts/engineering unit.

The computation of the sensitivity of the torsional strain gauge measurement is derived from the synthesis of the equations governing the electrical performance of the bridge circuit and the elastic behavior of circular shaft sections in torsion. The equation for computing the torsional sensitivity for a typical full bridge arrangement of strain gauge sensors (Figure 17) is as follows:

$$Ts = \left(8000 \bullet GF \bullet V_{exc} \bullet G_{amp} \bullet D_o\right) / \left(\pi \bullet G \bullet \left(D_o^4 - D_i^4\right)\right) \quad (33)$$

where:
GF = Strain gauge factor—typically very close to 2.0
V_{exc} = Excitation voltage applied to strain gauge bridge (volts)—typically fixed at 5 volts
G_{amp} = Amplifier gain setting for the telemetry transmitter
D_o = Outer diameter of strain gauged shaft section (inches)
D_i = Inner diameter of strain gauged shaft section (inches)
G = Shear modulus of steel (lbf/in^2)
T_S = Torque sensitivity (mV/in-lbf)

A further simplification of the above equation can be obtained if it is assumed that the instrumented shaft is composed of steel and has a solid cross-section.

$$Ts = 2.2069 \times 10^{-4} \bullet GF \bullet V_{exc} \bullet G_{amp} \,/\, D_o^3 \quad (34)$$

where:
GF = Strain gauge factor—typically very close to 2.0
V_{exc} = Excitation voltage applied to strain gauge bridge (volts)—typically fixed at 5 volts
G_{amp} = Amplifier gain setting for the telemetry transmitter
D_o = Outer diameter of strain gauged shaft section (inches)
T_S = Torque sensitivity (mV/in-lbf)

As one can see by examining Equation (33), in addition to selecting the appropriate location to mount the strain gauges (D_o), the choice of the appropriate telemetry gain (G_{amp}) is critical in determining the torsional sensitivity. Most modern digital telemetry systems permit the engineer to configure discreet values of gain over a range between 125 and 8000. It is the engineer's responsibility to choose the appropriate gain that optimizes the use of the dynamic input range of the data acquisition and/or recording hardware. A poor choice of gain can either result in an excessively noisy torque signal, or a signal that exceeds the dynamic range of the telemetry system and/or acquisition hardware (commonly known as signal clipping). Obtaining the maximum anticipated dynamic torque either from previous experience and/or analytical models can assist the engineer in making an educated selection of the appropriate telemetry gain.

When discussing the application of strain gauges for field measurements, it is imperative to comprehend how the use of this technology differs from that of a prepackaged sensor, such as an accelerometer. The use of strain gauges for field measurements often requires that the engineer develop a "custom" transducer design/setup. The use of the term "custom" reflects that, unlike a standard accelerometer whose accuracy/calibration and mounting/electrical requirements are determined by the manufacturer, the implementation of the gauge installation, calibration techniques, and signal conditioning hardware must be customized according to the shaft geometry, as well as other environmental factors (speed, moisture, etc.). In essence, once instrumented with strain gauges, the shaft becomes the transducer! Accordingly, to successfully instrument a shaft with strain gauges, the engineer must have a complete understanding of the measurement, space, and environmental requirements prior to beginning the test setup. Under normal circumstances, it is the authors' experience that torsional strain gauge measurements can be completed within one to two working days (setup, test, cleanup). The following section discusses a few of the basic engineering and logistical considerations associated with torsional strain gauge measurements.

As with any type of sensor, it is the engineer's responsibility to have a complete understanding of the performance and operational requirements of his/her equipment. Recognizing that field work is often performed under demanding conditions (limited time, noisy/inclement environment, etc.), it is especially important that the engineer allocates the appropriate time to accurately construct a written record of the test configuration, transducer and data acquisition setup/calibration data, so that he or she can competently process the data upon returning from the field. An unfortunate trend in field measurements, owing, in part, to the usage of computerized data acquisition systems that can provide "almost" instant results, is that engineers take fewer field notes. It is particularly important with torsional strain gauge testing, where the responsibility of the transducer calibration (the instrumented shaft) resides with the test engineer, that a thorough record of the supporting measurements, equipment settings, etc., exist to facilitate a confirmation/reassessment of the calibration data upon returning from the field.

Quite often, the most convenient place to strain gauge a shaft does not correspond to the optimal location to capture the maximum dynamic shaft torques. In general, for motor-driven trains, the maximum dynamic torques resulting from an excitation of the fundamental torsional twist mode of vibration will occur at, or near, the drive end of the motor rotor. Accordingly, this is usually the best place to locate strain gauges. As discussed in the previous section, the accuracy of the torsional strain gauge measurements is directly influenced by the elastic behavior of the shaft. Accordingly, to the extent possible, the engineer must maximize separation between the mounted gauges and any geometric discontinuities (keyways, radiuses, grooves, etc.) that will result in nonuniform torsional strains. When practical, it is also desirable to instrument solid shaft sections. Depending upon the wall thickness and the magnitude of the shaft torque, hollow shaft sections are predisposed to torsional warping, which can provide an erroneous measure of torque when interpreting the strain gauge signals in the context of classical elastic behavior for circular shaft sections. Finally, although it entails some extra work, it is always recommended to instrument the shaft with a full bridge complement of strain gauges, which are configured to electrically eliminate the influence of unwanted strains associated with shaft flexure.

It is always advisable to use manufacturer-recommended cleaning, adhesive, and environmental coating products for field installations. In general, most strain gauge setups are only required to function for a short period of time (rarely for durations lasting longer than a few weeks). Accordingly, fast curing, two-part adhesives will provide adequate performance for most field applications. Prior to adhering the gauges, the engineer must make certain that the shaft surface does not contain any nicks, dents, gouges, etc., within the gauge area that will not be removed via the strain gauge vendor's mechanical/chemical cleaning procedures. Upon occasion, the shaft may have to be manually rotated to expose a surface whose quality is suitable for the application of strain gauges. Finally, once adhered to the shaft, the engineer must thoroughly inspect the gauge to ensure that the adhesive provides a continuous bond between the underside of the gauge and the shaft surface. If the adhesion of the gauge to the shaft surface in any way appears to be suspect, it is best to mechanically remove it from the shaft and repeat the installation with a new gauge. When evaluating the integrity of the glue line between the strain gauge and the shaft surface, it should always be remembered that the adhesive is responsible for transferring the mechanical strain to the gauge's sensing grid, and therefore, should not be in question.

One of the selling points of many modern digital telemetry systems is that the engineer no longer has to be burdened with the field calibration of strain gauge sensors. This claim is primarily made owing to the fact that the front-end amplifiers that are incorporated into modern digital systems are much less susceptible to drift than are their analog predecessors. What this implies to the engineer is that he or she can take their theoretical calculations of torque sensitivity and reliably apply them directly to the acquired data to resolve torque. Unfortunately, this also means that the engineer is no longer performing any comprehensive checks to ensure that the strain gauge/telemetry system is functioning properly.

Recognizing again that field measurements are often made under demanding circumstances, regardless of the telemetry system in use (analog or digital), it is strongly recommended that the engineer also perform an electrical calibration (known as a shunt calibration) to confirm the sensitivity of the strain gauge setup. Using this method of calibration, one, or more, of the strain gauges in a bridge circuit is "shunted" with an external resistor (an external resistor placed in parallel with the strain gauge) and the resulting change in the telemetry system's output signal is recorded. Briefly stated, the act of shunting the strain gauge produces a readily quantifiable change in the combined resistance of the strain gauge/shunting resistor, which, utilizing the known calibration factor for the strain gauge (gauge factor), the resulting bridge circuit behavior can be equated to a mechanical strain. Although a complete derivation of the theory/procedure for strain gauge shunt calibrations is beyond the scope of this tutorial, it is important for readers who are unfamiliar with this practice to recognize that this is an accurate method to electronically verify that the strain gauge bridge and the associated telemetry hardware are working and configured correctly. It is the authors' experience that shunt calibration results should agree with the theoretical sensitivity of the torsional strain gauge bridge within 1 to 2 percent. For the interested reader, comprehensive procedures for performing shunt calibration are available in most strain gauge handbooks and/or from product literature provided by strain gauge vendors.

In most cases, the separation distance between the strain gauged shaft section and the rotor-mounted telemetry transmitter is less than one foot. Accordingly, for most applications, unshielded AWG 26 three-conductor cable can be used to connect the strain gauges to the telemetry input without predisposing the strain gauge setup to electromagnetic noise. Most modern telemetry systems permit the engineer to quantitatively evaluate the signal strength from the rotor-mounted transmitter. Prior to establishing a permanent location for the stationary receiving antenna, it is always prudent to move the receiving antenna around the circular envelope that will be swept by the rotating transmitter to evaluate the signal strength. Depending upon the diameter of the shaft section with the mounted transmitter, as well as the proximity of any fixed enclosures around the shaft, it is possible that locating the receiving antenna too close to the transmitter will result in an excessively strong carrier signal that will overdrive the receiver's circuit, resulting in an intermittent loss of telemetry data.

Recognizing that the strain gauges, wiring, and telemetry transmitter are attached to a rotating shaft, it is critical that all these components, and their associated electrical connections, are mechanically secured. It is good practice to fasten all wiring to the shaft along their entire lengths using a combination of strapping tape and wire ties. Wires that are left unsecured will inevitably cause problems by either snagging a fixed object and/or fatiguing. On several occasions, loose/unsecured wires have also been found to be the culprit behind an undesirably noisy strain gauge signal.

STRAIN GAUGE TESTING OF 66,000 HP AIR COMPRESSOR

The practical implementation of strain gauge testing, as well as the effectiveness of the presented analytical procedure, was recently demonstrated when the authors ran strain gauge tests on the 66,000 hp air compressor described previously. Additionally, three other compressors at the same site also underwent torsional analysis using the procedure described herein and were also subse-

quently tested using strain gauges. Although the strain gauge tests validated the analytical procedure for all four machines, this discussion will focus on the testing of the air compressor only.

For all four compressors, the test setup was designed to capture the requisite mechanical and electrical data to measure/confirm levels of torsional vibration on the low-speed shafting occurring during starting. A total of seven measurements was made during each monitored startup. An overview of acquired measurements is presented in Table 4.

Table 4. Measurements Taken During Strain Gauge Testing.

Measurement Number	Sensor Type	Purpose
1	Tachometer	Measurement of shaft rotation on low speed shafting used to synchronize all measurements with rotational speed
2	Torsional Strain Gage	Measurement of torsional strain at two diametrically-opposite locations on shaft to deduce dynamic torque
3	Current	Measurement of motor current (Phase A) from switchhouse current transformer
4	Current	Measurement of motor current (Phase B) from switchhouse current transformer
5	Current	Measurement of motor current (Phase C) from switchhouse current transformer
6	Voltage	Measurement of differential motor voltage (Phases A-B) from switchhouse power transformer
7	Voltage	Measurement of differential motor voltage (Phases C-B) from switchhouse power transformer

The low-speed shafting on each of the compressor trains was instrumented with identical arrangements of two 45 degree rosette strain gauges to dynamically measure the torsional strains. As is illustrated in Figure 18, each shaft was instrumented with strain gauge rosettes at two diametrically opposite locations around its circumference. These gauges were wired in a Wheatstone full bridge sensing circuit to measure only pure torsional strain. The placements for the strain gauges were carefully selected to avoid any discontinuities in the torsional strain field arising from keyways, steps, splines, grooves, etc. The shaft diameter at each gauged location was field checked by plant personnel. The measured shaft diameters and mechanical properties of the shafting (in all cases steel) were used to compute the corresponding shaft torques from the strain measurements. In the testing of the air compressor, the strain gauges were located at the coupling end of the motor shaft.

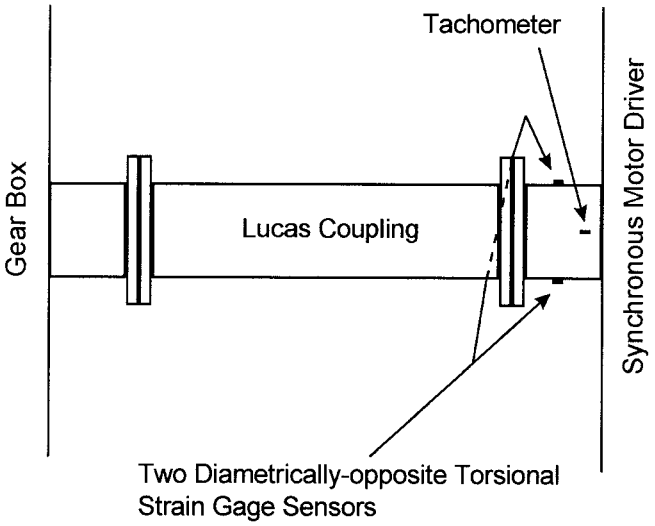

Figure 18. Strain Gauge Layout for Air Machine Testing.

A telemetry system was used to supply a regulated input voltage (5 VDC) for each of the full bridge strain gauge circuits. This transmitter unit, affixed to the rotating shaft/coupling, converted the conditioned analog strain gauge signals to 14 bit digital frequency-modulated (FM) radio signals that were being monitored by a stationary receiving unit. The receiving unit demodulated the radio signals to produce analog signals, prior to acquisition. The frequency response of the telemetry system is approximately 800 Hz.

Manufacturer-recommended mounting, adhesion, and wiring products and procedures were utilized to install the strain gauges. Also, prior to test, industry standard calibration procedures were used to verify the functionality of each strain gauge circuit, as well as to calibrate the transmitter gain.

As is illustrated in Figure 18, an optical tachometer measurement was made on the low-speed shafting (between the motor and gearbox) of each compressor train. The tachometer hardware provided an analog time tracking loop (TTL) signal when a stationary light beam reflected off a reflective tape strip, adhered to the rotating shaft, exceeded a threshold intensity. The resulting square wave signals (pulse train) provided time-based references to facilitate the synchronization of the measured torque and electrical data with the shaft speed.

The authors measured the electrical currents on all three phases of each motor's current transformer (CT) using AC current clamps. These clamps, themselves also current transducers, provided a voltage signal that was proportional to the measured CT amperage (10 mV/amp). To minimize the fixed errors associated with this type of measurement device, multiple turns of the load line were passed through each of the clamps, thus increasing the dynamic range of the measurements.

The differential electrical voltages on each motor's power transformer (PT) were measured using a voltage divider circuit. These circuits, a serial arrangement of resistors, provided a voltage signal that was proportional to the measured PT voltage (43.1 mV/volt). Each of the voltage measurements (Phases A and C) was made with respect to Phase B.

The authors utilized a 16-channel, computer-based data acquisition system to record and store the data for each test. The hardware was configured to provide true simultaneous acquisition. The sampling rate for all channels was set to 1024 samples per second. This sampling rate provided sufficient frequency resolution (400 Hz) in the acquired data to accurately capture the dynamic behavior of the four compressors during testing. The duration of each acquisition window was approximately two seconds. By configuring this hardware to take a continuous stream of two second acquisitions, as much as several minutes of uninterrupted dynamic data could be logged for each test.

As a backup to the data acquisition unit, an analog tape recorder was also configured to record the test data. Each tape channel was configured with an amplifier attenuation of 10. The tape recording speed was set to 1-7/8 to provide approximately 5 kHz frequency response.

Dynamic mechanical and electrical data were collected during the synchronous motor startup transient for each of the four compressor trains. After an initial canvassing of all the transient startup data, representative time-based windows were selected for further processing. The length of each data window corresponded to a period of time beginning just prior to energization of the motor and lasting until the motor reached its synchronous speed (1800 rpm). Prior to processing the data from each test, the static (pretest) sensor "DC" levels were subtracted from each dynamic signal. Accordingly, for example, the absolute torque values are referenced to the residual torques that existed prior to test.

The results of the strain gauge testing performed on the 66,000 hp air compressor are provided in Figures 19 and 20. Both figures show the measured torque and speed at the motor shaft as a function of time. It is easily seen that, qualitatively, these figures

are very similar to the analytically predicted curve of Figure 10. That is, the torque remains relatively steady up until the point where resonance with the first natural frequency is achieved. At that point, the response slowly builds up until it reaches a peak and then it slowly drops down to a relatively steady value.

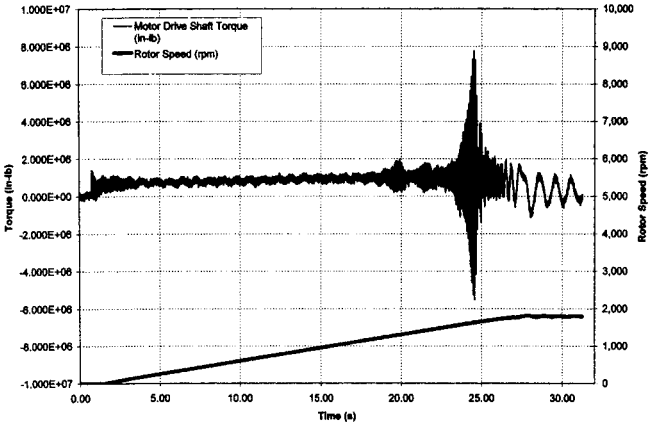

Figure 19. Air Compressor Response Measured by Strain Gauges.

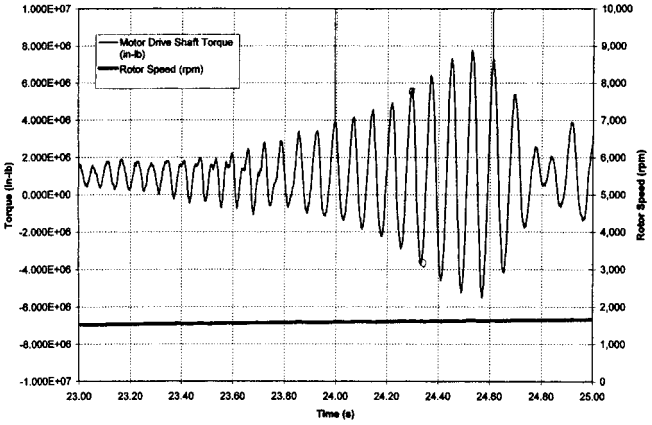

Figure 20. Air Compressor Resonance Zone Measured by Strain Gauges.

Remembering that the per unit torque for this machine is 2.31E6 in-lb, it is seen that the peak torque observed in testing (3.349 pu) is only about 70 percent of the analytical value (4.811 pu). This indicates that the original analysis had erred on the conservative side, which is precisely what had been hoped.

After the test results were obtained, the analytical model was "tuned" in an attempt to provide the best possible agreement with the test data. The purpose of doing this was to obtain an improved estimate for the allowable number of starts. This procedure was initiated by first employing the measured electrical data to calculate the motor's actual average and pulsating torque versus speed curves for the tested conditions. These were then substituted for the theoretical curves in the analytical model and the transient analysis was rerun. The generic damping coefficient, which had previously been set at a value of 2.0 percent of critical, was then iteratively varied until the analytical response at the motor provided the best match with the test results. Using trial and error, the damping coefficient that yielded the best match was found to be 4.8 percent of the critical value. Since this was almost 2.5 times the damping that had originally been applied, this also indicated that the original analysis was conservative.

Using the empirically determined damping factor of 4.8 percent, the response plots were then regenerated for all shafts of interest. The rigorous life prediction procedure described earlier was then utilized to obtain a revised prediction for the number of starts each shaft could withstand. As was the case with the original analysis, the pinion shaft was again found to be the weak link. However, the allowable number of starts, which had been 5442, was found to increase to 28,773, almost a fivefold increase. Similarly, the allowable number of starts for the motor shaft, which had previously been found to be 7307, was found to increase to 35,564.

A comparison of the analytically predicted and empirically observed values of all the air machine's relevant parameters is provided in Table 5. Examination of this table leads to the following conclusions:

Table 5. Comparison of Air Compressor Analytical and Measured Results.

Air Compressor	Analysis	Test
Natural Frequency (Hz)	14	13.21
Time at Resonance (sec)	21.7	24.53
Speed at Resonance (RPM)	1608	1648
Motor Average Torque at Resonant Speed (PU)	0.565	0.492
Motor Pulsating Torque at Resonant Speed (PU)	0.4	0.461
Shaft Containing Strain Gages	Motor	Motor
Shaft Max. Torque (PU)	4.811	3.349
Shaft Min. Torque (PU)	-3.848	-2.386
Shaft Cycle Torque (PU)	4.33	2.868
Amplification Factor at Resonance	12.03	7.27
"Weak Link" Shaft	Pinion	Pinion
Allowable No. of Starts	5442	28773

- For the most basic parameters (resonant frequency, time at resonance, and speed at resonance), the agreement is excellent. This provides a solid validation of the transient torsional analysis.
- In spite of the fact that the motor's actual pulsating torque at resonance was somewhat higher than the theoretical value, the peak shaft torques were significantly lower than the calculated values. This clearly shows that the system damping is substantially higher than the originally assumed value of 2.0 percent.
- Most importantly, the nearly fivefold increase in allowable number of starts proves that the advocated analytical procedure provides ample margin and is, thereby, a highly useful design tool.

It is, therefore, seen that the strain gauge testing has validated the analytical procedure presented herein. Although this procedure is less conservative than those that are currently being used in most organizations, it still provides ample margin for design purposes.

CONCLUSION

A comprehensive procedure for the analysis and testing of torsional vibration in turbomachines being driven by synchronous motors has been presented. The methodology is general enough that it should be applicable to any synchronous motor-driven turbomachine. The key points that should be emphasized are as follows:

- A thorough torsional vibration analysis should always be included as an integral part of the design process for any turbomachine.
- Turbomachines driven by synchronous motors need to be handled with extra caution due to the large pulsating torques they generate during starting.
- The traditional method for calculating shaft fatigue lives (stress-life method) is overconservative. The strain-life theory provides a much better calculation tool.
- There is currently a tremendous amount of confusion regarding the proper manner in which fatigue strength reduction factors should be applied. The method presented herein attempts to resolve that confusion.

• The traditional torsional vibration stress safety factor of 2.0, while being perfectly appropriate for steady-state situations, is too conservative for transient analyses.

• Because of the log-log nature of the strength versus life curve, small errors in calculated strengths can lead to large errors in life prediction.

• On machines of critical importance, the analytical procedure should be supplemented with a testing program, employing strain gauges.

• Torsional vibration analysis, fatigue life analysis, and strain gauge testing are not exact sciences that can be performed by just anybody. The importance of the skill, judgment, and experience of the engineer involved should never be underestimated.

REFERENCES

Anwar, I. and Colsher, R., 1979, "Computerized Time Transient Torsional Analysis of Power Trains," ASME Paper 79-DET-74.

Banantine, J. A., Comer, J. J., and Handrock, J. L., 1990, *Fundamentals of Metal Fatigue Analysis*, Englewood Cliffs, New Jersey: Prentice Hall.

Bogacz, R., Irretier, H., and Szolc, T., 1990, "Analysis of Transient Torsional Vibrations in the Rotor Machine Using a Hybrid Model," *Proceedings of the Third International Conference on Rotordynamics*, IFToMM, Lyon, France, pp. 207-211.

Boyer, H., 1986, *Atlas of Fatigue Curves*, ASTM.

Chen, W. J., 1995, "Torsional Vibrations of Synchronous Motor Driven Trains Using P-Method," ASME Journal of Vibration and Acoustics, pp. 152-160.

Chen, H. M., McLaughlin, D. W., and Malanoski, S. B., 1983, "A Generalized and Simplified Transient Torque Analysis for Synchronous Motor Drive Trains," *Proceedings of the Twelfth Turbomachinery Symposium*, Turbomachinery Laboratory, Texas A&M University, College Station, Texas, pp. 115-119.

Corbo, M. A. and Malanoski, S. B., 1996, "Practical Design Against Torsional Vibration," *Proceedings of the Twenty-Fifth Turbomachinery Symposium*, Turbomachinery Laboratory, Texas A&M University, College Station, Texas, pp. 189-222.

Draminsky, P., 1948, "Crankshaft Damping," Proceedings of the Institution of Mechanical Engineers, pp. 416-432.

Evans, B. F., Smalley, A. J., and Simmons, H. R., 1985, "Startup of Synchronous Motor Drive Trains: The Application of Transient Torsional Analysis to Cumulative Fatigue Assessment," ASME Paper 85-DET-122.

Grgic, A., Heil, W., and Prenner, H., 1992, "Large Converter-Fed Adjustable Speed AC Drives for Turbomachines," *Proceedings of the Twenty-First Turbomachinery Symposium*, Turbomachinery Laboratory, Texas A&M University, College Station, Texas, pp. 103-112.

Jackson, M. C. and Umans, S. D., 1980, "Turbine–Generator Shaft Torques and Fatigue: Part III—Refinements to Fatigue Model and Test Results," IEEE Transactions on Power Apparatus and Systems, pp. 1259-1268.

Joyce, J. S., Kulig, T., and Lambrecht, D., 1978, "Torsional Fatigue of Turbine Generator Shafts Caused by Different Electrical System Faults and Switching Operations," IEEE PES Winter Meeting, New York, New York.

Juvinall, R., 1967, *Engineering Considerations of Stress, Strain, and Strength*, New York, New York: McGraw-Hill, Inc.

Manson, S. S., Nachtigall, A. J., Ensign, C. R., and Freche, J. C., 1965, "Further Investigation of a Relation for Cumulative Fatigue Damage in Bending," ASME Journal of Engineering for Industry, pp. 25-35.

Miner, M. A., 1945, "Cumulative Damage in Fatigue," ASME Journal of Applied Mechanics, pp. A159-A164.

Mischke, C. R., 1982, "Predicting Fatigue Endurance Strengths for High- and Low-Cycle Fatigue," ASME Journal of Mechanical Design, pp. 653-660.

Mruk, G., Halloran, J., and Kolodziej, R., 1978, "New Method Predicts Startup Torque—Part 1: Analytical Model," *Hydrocarbon Processing*, pp. 181-186.

Peterson, R. E., 1974, *Stress Concentration Factors*, New York, New York: John Wiley and Sons.

Pollard, E. I., 1980, "Synchronous Motors … Avoid Torsional Vibration Problems," *Hydrocarbon Processing*.

Shannon, J. F., 1935, "Damping Influences in Torsional Oscillation," Proceedings of the Institution of Mechanical Engineers, pp. 387-435.

Shigley, J. E. and Mischke, C. R., 1986, *Standard Handbook of Machine Design*, New York, New York: McGraw-Hill, Inc.

Shigley, J. E. and Mischke, C. R., 1989, *Mechanical Engineering Design*, Fifth Edition, New York, New York: McGraw-Hill, Inc.

Simmons, H. R. and Smalley, A. J., 1984, "Lateral Gear Shaft Dynamics Control Torsional Stresses in Turbine-Driven Compressor Train," ASME Journal of Engineering for Gas Turbines and Power, pp. 946-951.

Smalley, A. J., 1983, "Torsional System Damping," *Proceedings of the Seventh Annual Meeting of the Vibration Institute*, The Vibration Institute, Houston, Texas.

Sohre, J. S., 1965, "Transient Torsional Criticals of Synchronous Motor Driven, High-Speed Compressor Units," ASME Paper 65-FE-22.

Szenasi, F. R. and von Nimitz, W. W., 1978, "Transient Analyses of Synchronous Motor Trains," *Proceedings of the Seventh Turbomachinery Symposium*, Turbomachinery Laboratory, Texas A&M University, College Station, Texas, pp. 111-117.

Wachel, J. C. and Szenasi, F. R., 1993, "Analysis of Torsional Vibrations in Rotating Machinery," *Proceedings of the Twenty-Second Turbomachinery Symposium*, Turbomachinery Laboratory, Texas A&M University, College Station, Texas, pp. 127-151.

Walker, D. N., Adams, S. L., and Placek, R. J., 1981, "Torsional Vibration and Fatigue of Turbine-Generator Shafts," IEEE Transactions on Power Apparatus and Systems, pp. 4373-4380.

Wright, J., 1975, "Large Synchronous Motor Drives: A Review of the Torsional Vibration Problem and Its Solution," Koppers Company, Inc., Baltimore, Maryland.

BIBLIOGRAPHY

Artilles, A., Smalley, A. J., and Lewis, P., 1975, "Mill Drive System Vibrations," Proceedings of the National Conference on Power Transmission, Chicago, Illinois.

Brown, R. N., 1960, "A Torsional Vibration Problem as Associated with Synchronous Motor Driven Machines," ASME Journal of Engineering for Power, pp. 215-220.

De Choudhury, P., 1986, "Torsional System Design Relative to Synchronous Motor Start-Up with a Variable Frequency Power Supply System," *Proceedings of the Second International Conference on Rotordynamics*, IFToMM, Tokyo, Japan, pp. 325-328.

Ehrich, F. F., 1992, *Handbook of Rotordynamics*, New York, New York: McGraw-Hill.

Eshleman, R. L., 1977, "Torsional Vibration of Machine Systems," *Proceedings of the Sixth Turbomachinery Symposium*, Turbomachinery Laboratory, Texas A&M University, College Station, Texas, pp. 13-22.

Grover, H., 1954, *The Fatigue of Metals and Structures*.

Iwatsubo, T., Yamamoto, Y., and Kawai, R., 1986, "Startup Torsional Vibration of Rotating Machine Driven by Synchronous Motor," *Proceedings of the Second International Conference on Rotordynamics*, IFToMM, Tokyo, Japan, pp. 319-324.

Jackson, M. C., Umans, S. D., Dunlop, R. D., Horowitz, S. H., and Parikh, A. C., 1979, "Turbine-Generator Shaft Torques and Fatigue: Part I—Simulation Methods and Fatigue Analysis," IEEE Transactions on Power Apparatus and Systems, pp. 2299-2307.

Ker Wilson, W., 1956, *Practical Solution of Torsional Vibration Problems*, Volumes 1, 2, and 3, New York, New York: John Wiley and Sons.

Manson, S. S., 1966, "Interfaces Between Fatigue, Creep, and Fracture," Lewis Research Center, Cleveland, Ohio.

Manson, S. S., Nachtigall, A. J., and Freche, J. C., 1961, "A Proposed New Relation for Cumulative Fatigue Damage in Bending," ASTM Proceedings, pp. 679-703.

Mruk, G. K., 1978, "Compressor Response to Synchronous Motor Startup," *Proceedings of the Seventh Turbomachinery Symposium*, Turbomachinery Laboratory, Texas A&M University, College Station, Texas, pp. 95-101.

Nelson, D. V. and Sheppard, S. D., 1995, "Fatigue and Fracture Estimation for Metallic Components: Some Current Methods and Future Developments," ASME Journal of Mechanical Design, pp. 121-127.

Nestorides, E., 1958, *A Handbook on Torsional Vibration*, London, England: Cambridge University Press.

Pollard, E. I., 1967, "Torsional Response of Systems," ASME Journal of Engineering for Power, pp. 316-324.

Smalley, A. J., 1974, "Transient Torsional Vibration," Mechanical Technology Incorporated, Latham, New York.

Thames, P. B. and Heard, T. C., 1959, "Torsional Vibrations in Synchronous Motor-Geared-Compressor Drives," AIEE Transactions, pp. 1053-1056.

Vance, J. M., 1988, *Rotordynamics of Turbomachinery*, Chapter 3, New York, New York: John Wiley and Sons.

Williams, P. N., McQuin, N. P., and Buckland, J. E., 1989, "The Importance of Complete Drive Train Analysis for Brushless Salient Pole Motor Drives," *Proceedings of the Fourth International Conference on Electrical Machines and Drives*, IEE-England, pp. 210-214.

ACKNOWLEDGEMENTS

The authors would like to recognize the contributions of Stan Malanoski of No Bull Engineering, Urs Baumann of Sulzer Turbo, John Cimusz of Motiva Enterprises, Mark DeBlock of General Electric, and Stan Polonski of Praxair who all provided valuable suggestions and feedback during the development of the analysis procedure presented herein. They would also like to thank Dr. Dara Childs and Ken Beckman of the Turbomachinery Symposium Advisory Committee for their invaluable feedback and encouragement.